CHIRAL MAGNETIC EFFECT & RELATIVISTIC ISOBAR COLLISIONS

徐浩洁

湖州师范学院

QCD物理研讨会暨基金委重大项目“量子色动力学的相结构和新颖拓扑效应研究”年度学术交流会

2022.07.28-31

Outline

I. Introduction

II. Search for the CME with the spectator/participant plane method

III. Search for the CME with Relativistic isobar collisions

IV. Probing the neutron skin thickness with relativistic isobaric collisions

V. Summary

I. Introduction

Relativistic heavy ion collisions

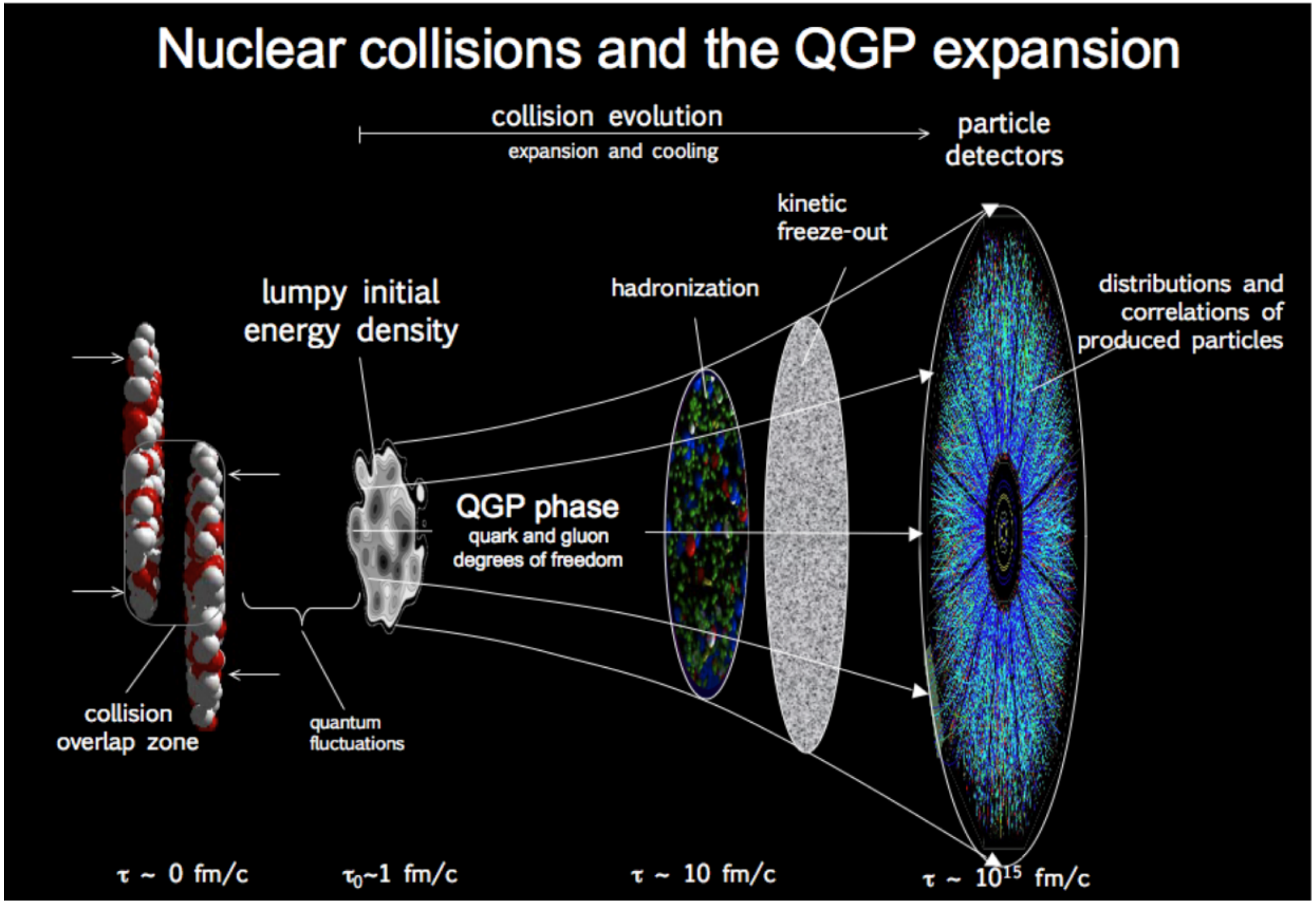

Chiral Magnetic Effect

D.E. Kharzeev et al. / Nuclear Physics A 803 (2008) 227–253

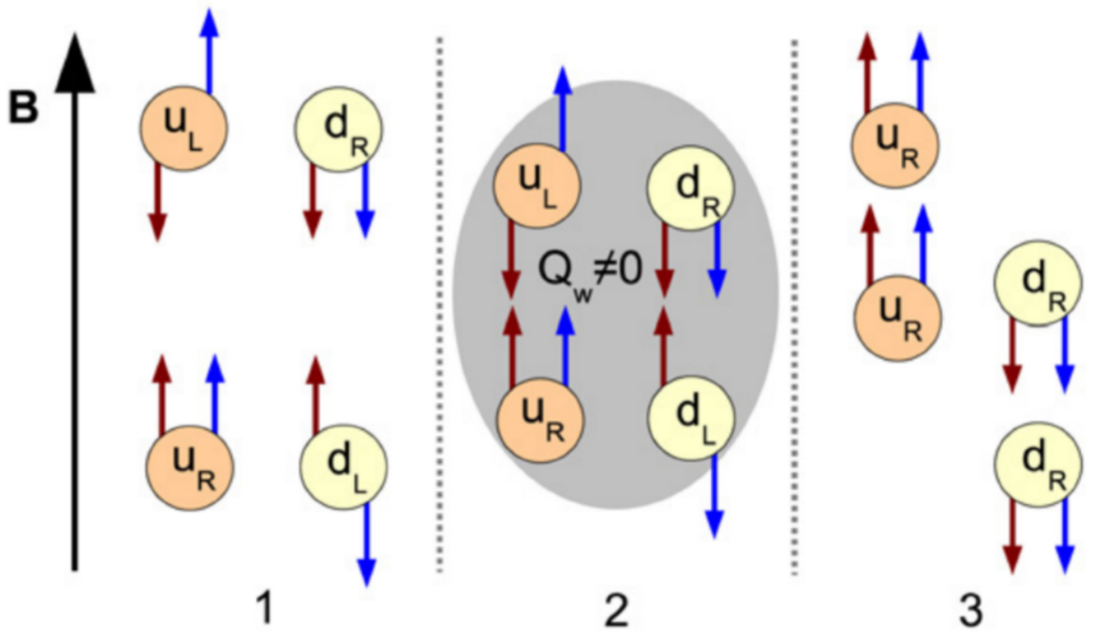

$$\mathbf{J}_{\mathbf{cme}} = \sigma_5 \mathbf{B} = \left(\frac{(Qe)^2}{2\pi^2} \mu_5 \right) \mathbf{B},$$

D. Kharzeev, PPNP88, 1(2016)

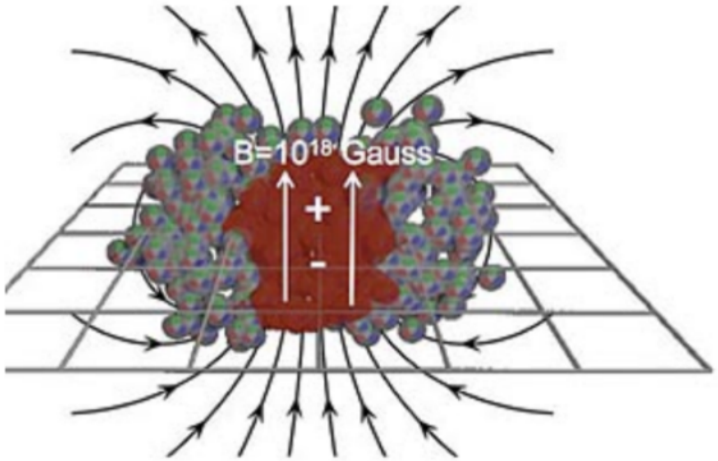

$$eB \sim m_\pi^2$$

- Magnetic field

$$Q_w = \frac{g^2}{32\pi^2} \int d^4x \, F^a_{\mu\nu} \tilde{F}^{\mu\nu}_a$$

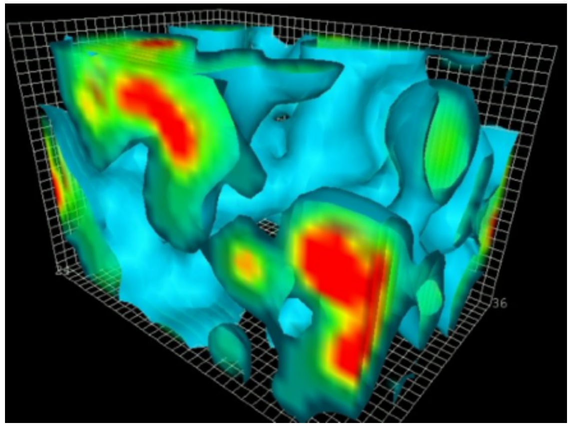

- QCD Vacuum: Fluctuations of topological charge

The gamma correlator

The gamma correlator: EBE charge separation wrt. reaction plane

$$\frac{dN_\pm}{d\phi} \propto 1 + 2v_1\cos(\phi-\Psi_{\rm RP}) + 2v_2\cos[2(\phi-\Psi_{\rm RP})] + ... + 2a_\pm\sin(\phi-\Psi_{\rm RP}) + ...,$$

$$\begin{aligned}\gamma \equiv \langle\cos(\phi_\alpha+\phi_\beta-2\Psi_{\rm RP})\rangle &= \langle\cos\Delta\phi_\alpha\,\cos\Delta\phi_\beta\rangle - \langle\sin\Delta\phi_\alpha\,\sin\Delta\phi_\beta\rangle \\ &= [\langle v_{1,\alpha}v_{1,\beta}\rangle + B_{\rm IN}] - [\langle a_\alpha a_\beta\rangle + B_{\rm OUT}] \\ &\approx -\langle a_\alpha a_\beta\rangle + [B_{\rm IN} - B_{\rm OUT}],\end{aligned}$$

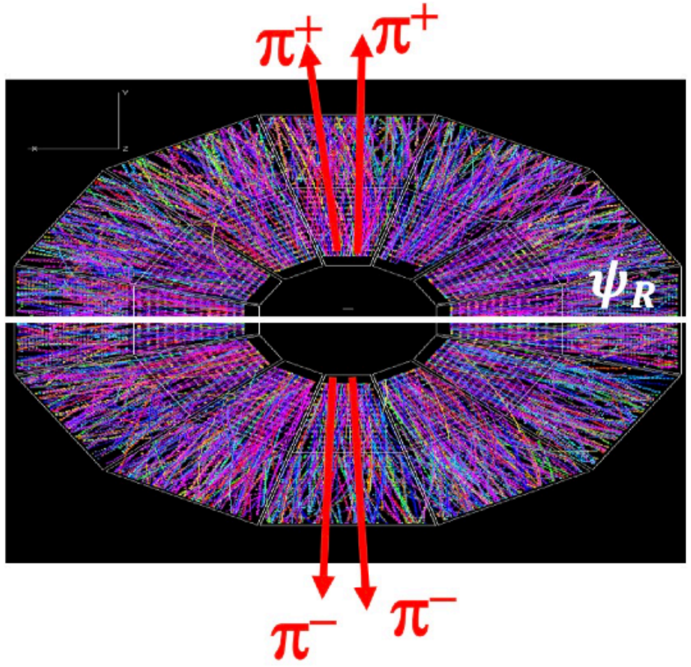

$\gamma_{+-,-+} > 0$ or $\gamma_{OS} > 0$

$\gamma_{++,--} < 0$ or $\gamma_{SS} < 0$

$\Delta\gamma > \equiv \gamma_{OS} - \gamma_{SS} > 0$

Experimental measurements

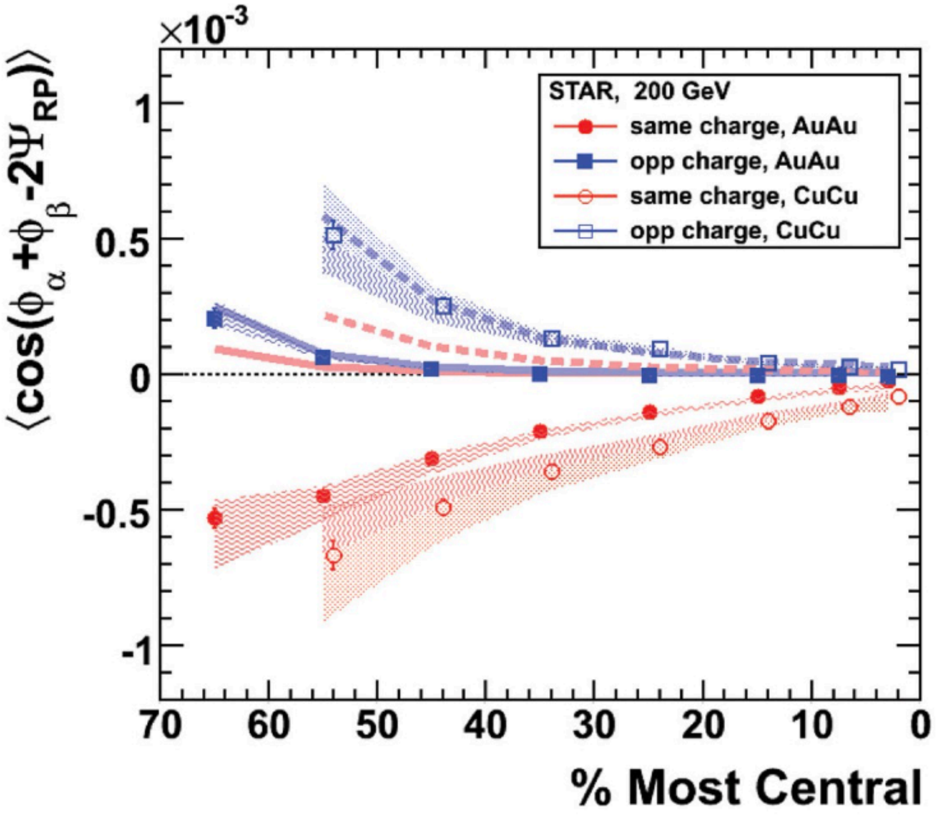

STAR, PRL103, 251601 (2009)

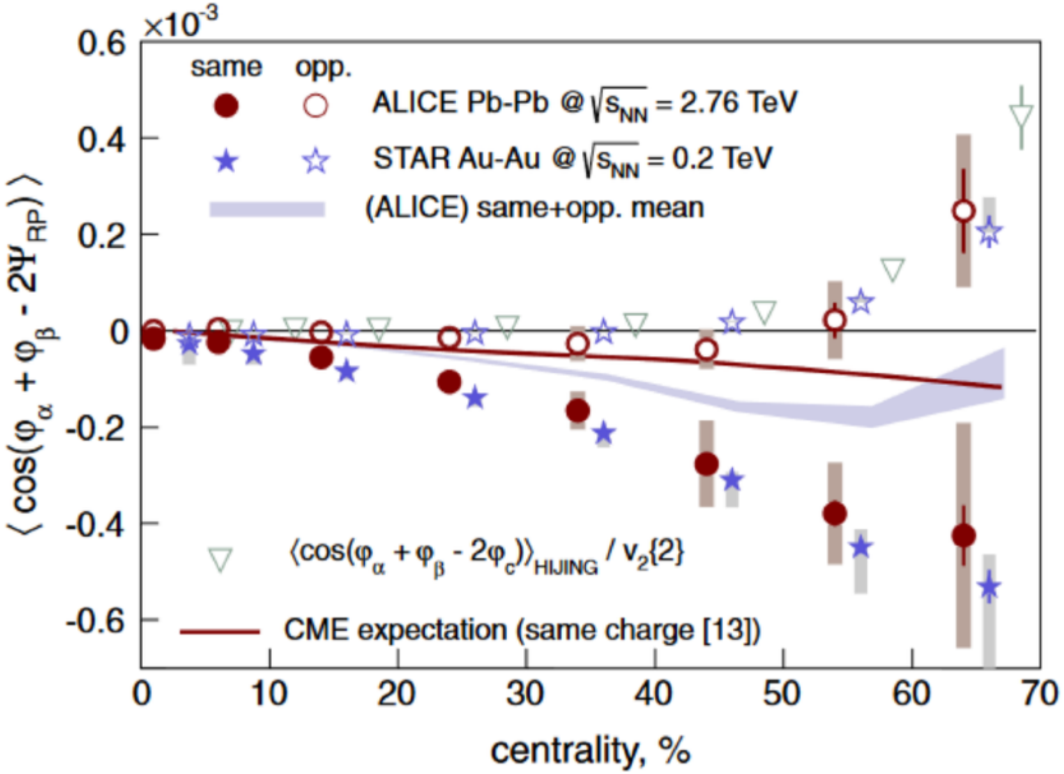

ALICE, PRL110, 012301(2013)

A clear signal compatible with EBE charge separation wrt. reaction plane is observed.
However…..

Background issues

Schlichting, PRC83(2011)
Bzdak, PRC81(2010)
Wang, PRC81(2010)

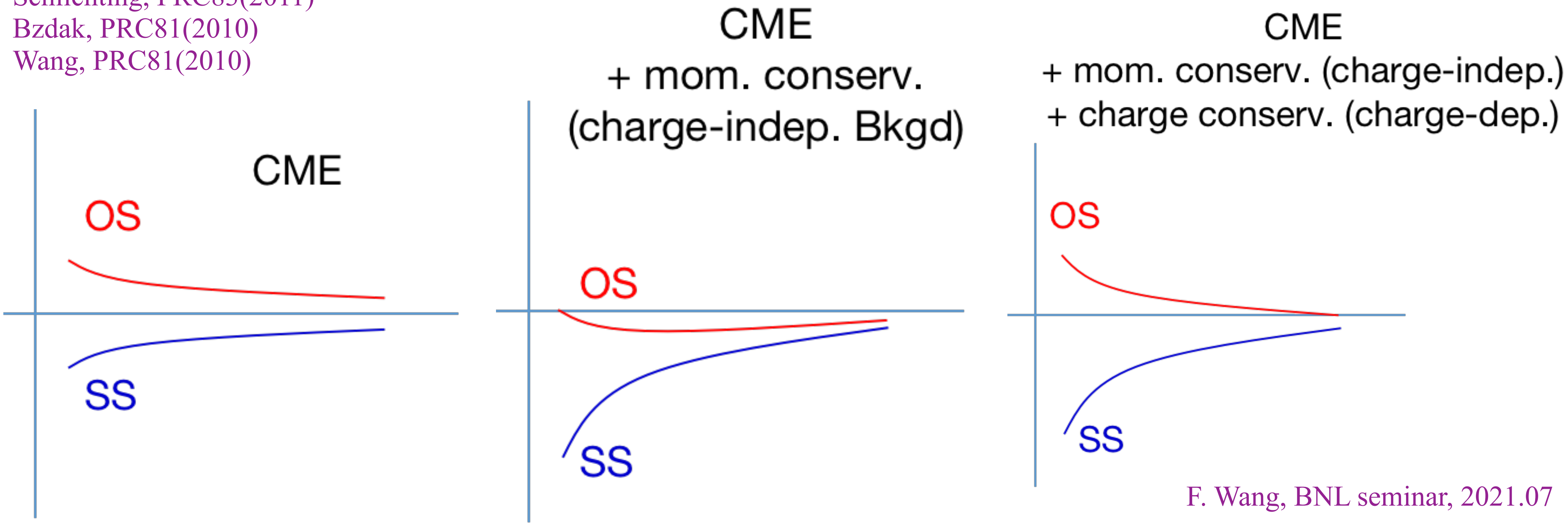

F. Wang, BNL seminar, 2021.07

$$\Delta\gamma = \gamma_{\mathrm{OS}} - \gamma_{\mathrm{SS}}$$

- Momentum conservation: charge-independent background, same contributions for γ_{OS} and γ_{SS}.
- Charge conservations: change-dependent background, can not be removed with $\Delta\gamma$

Charge conservation

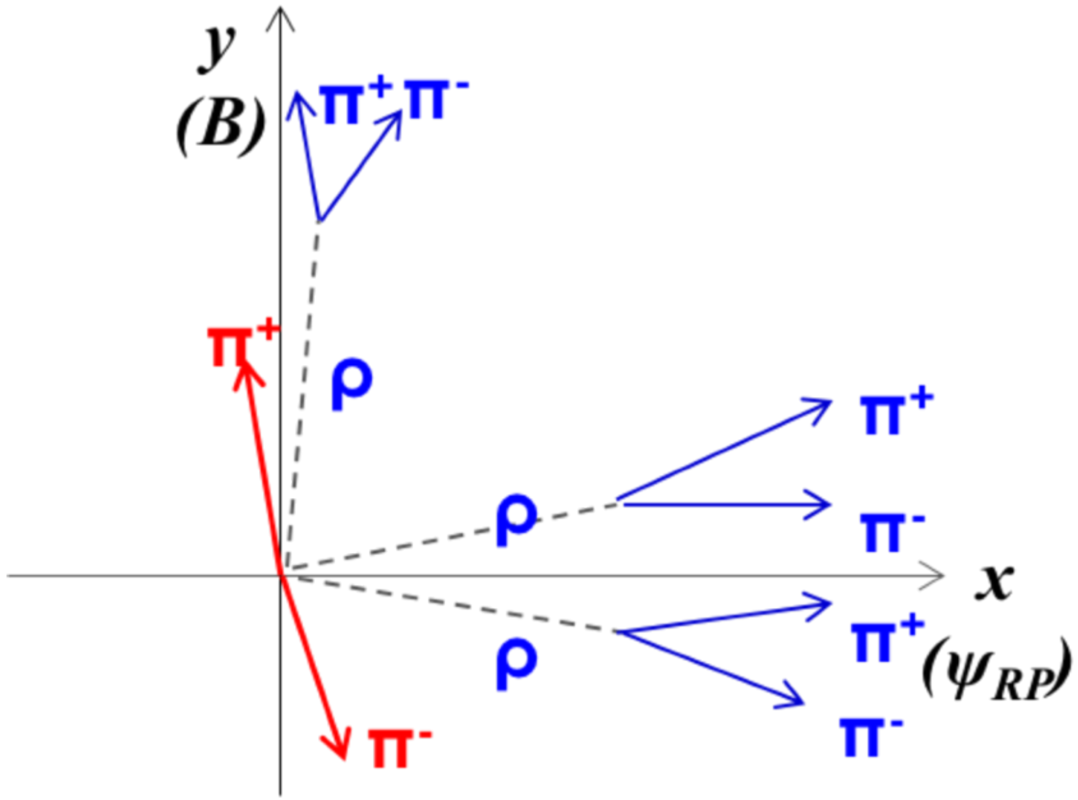

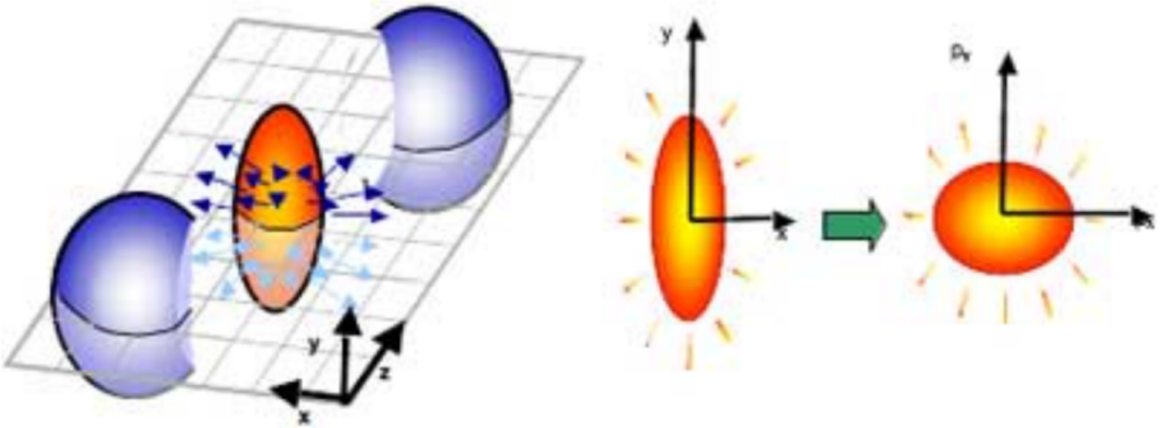

$$\frac{dN}{d\varphi} = N(1 + 2\sum_{n} v_n cos[n(\varphi - \Psi_n])$$

$v_2 = \langle cos2(\varphi - \Psi_2)\rangle$: elliptic flow

$$\Delta\gamma_{\rm bkg} = \langle\cos(\varphi_\alpha + \varphi_\beta - 2\Psi_{RP})\rangle = \frac{N_{\rm cluster}}{N_\alpha N_\beta} \times \langle\cos(\varphi_\alpha + \varphi_\beta - 2\Psi_{\rm cluster}) \times \cos(2\Psi_{\rm cluster} - 2\Psi_{RP})\rangle$$

Small system measurements

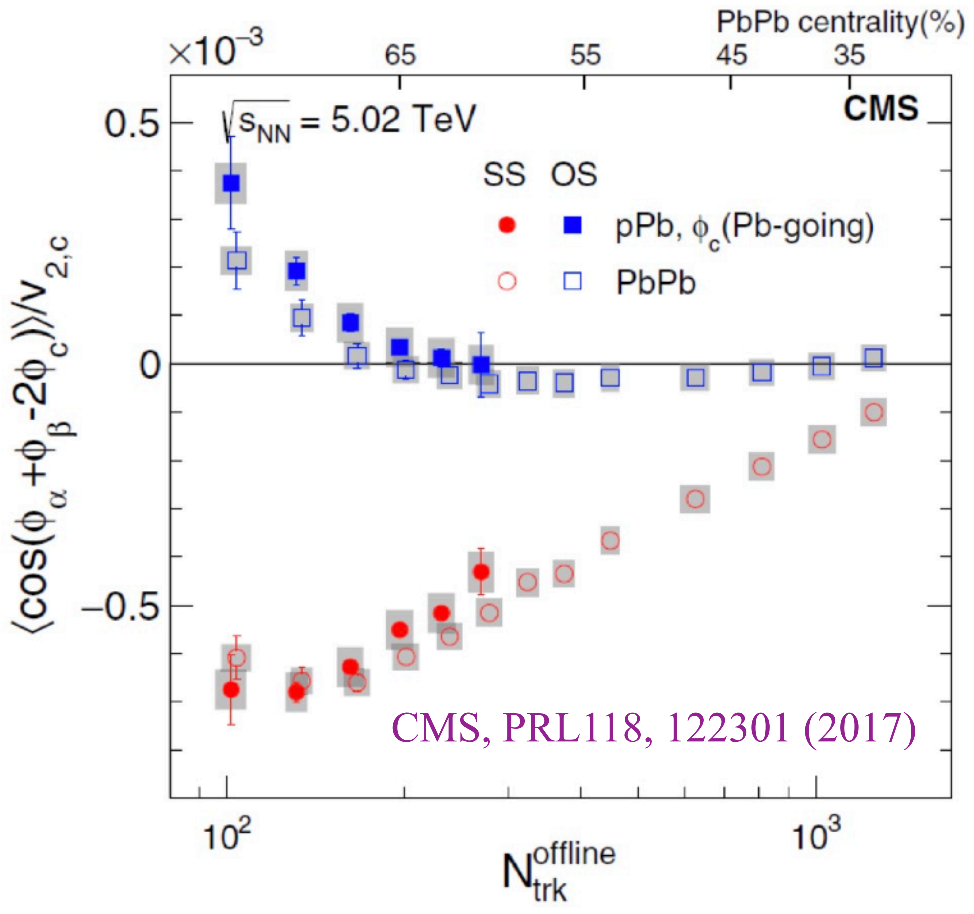

CMS, PRL118, 122301 (2017)

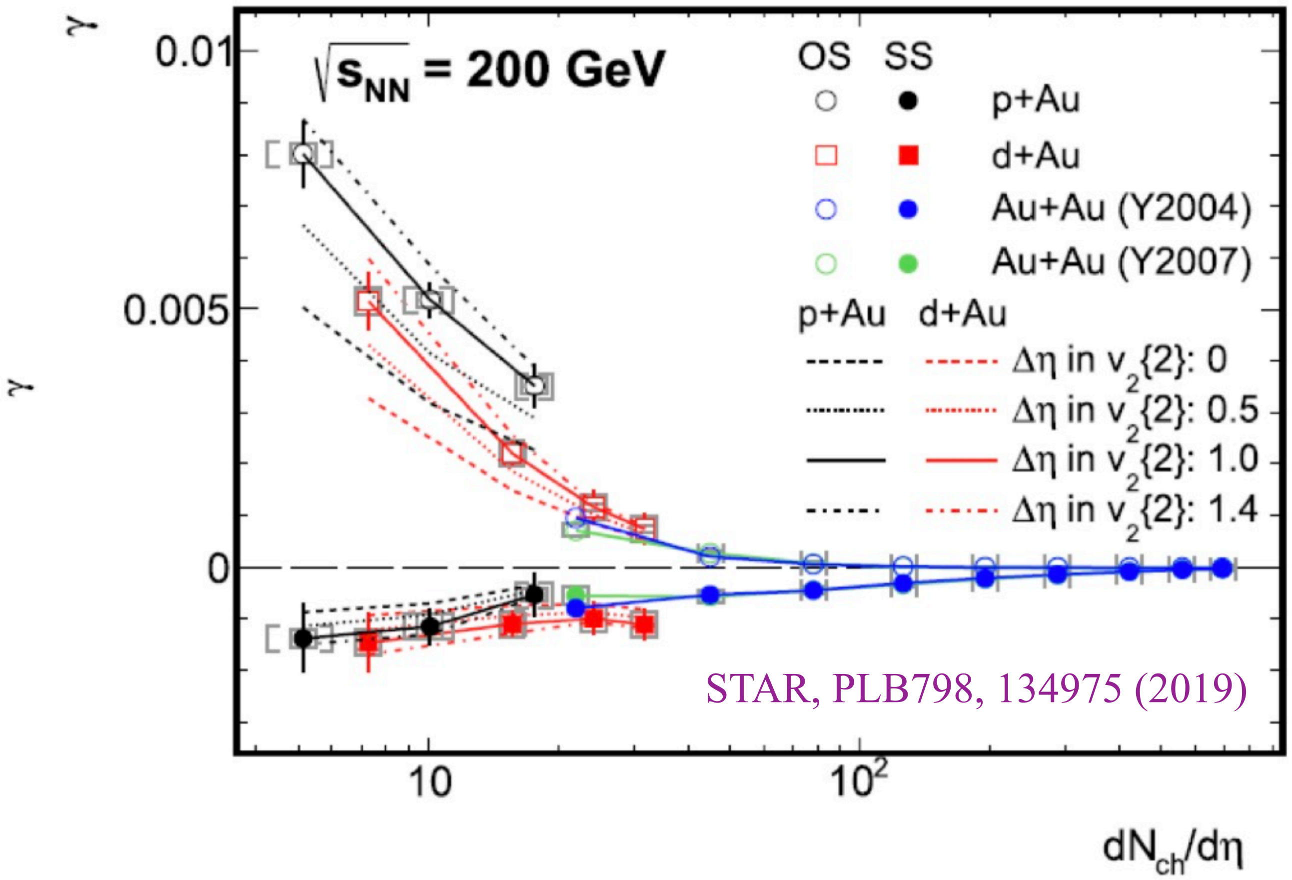

STAR, PLB798, 134975 (2019)

Large $\Delta\gamma$ in small systems indicate large background in CME measurements

II. Search for the CME with spectator/participant plane method

SP/PP method

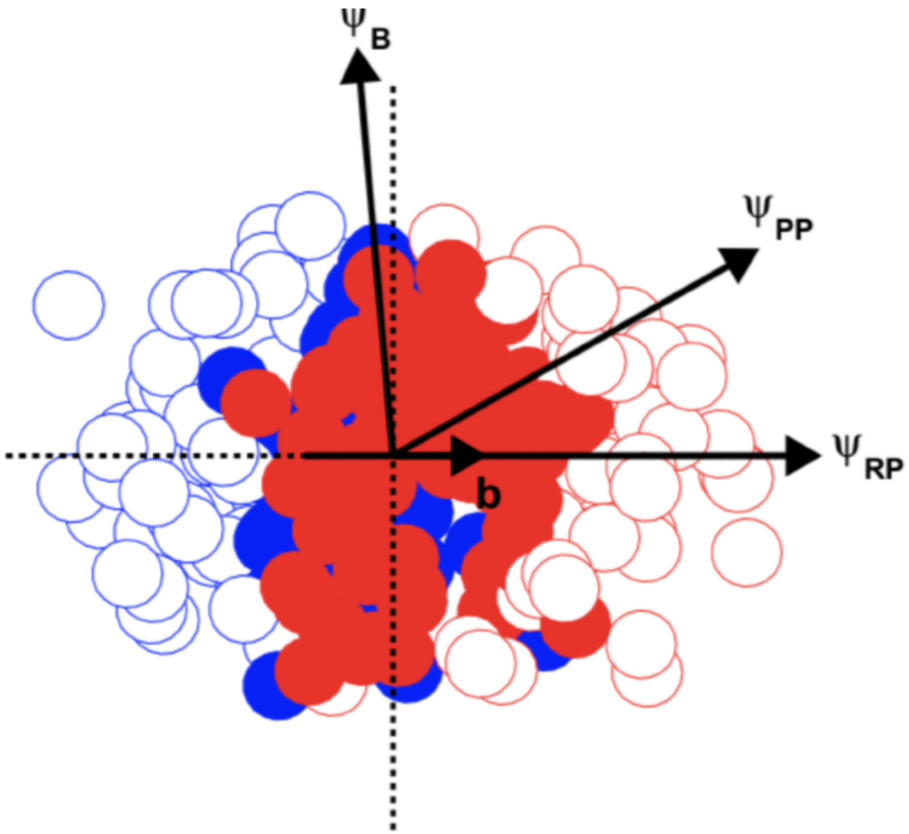

“Varying the chiral magnetic effect relative to flow in a single nucleus-nucleus collision”

Factorization

HJX, et al, CPC42, 084103 (2018)

$$a^{\mathrm{PP}}_{\epsilon_2} \equiv \epsilon_2\{\psi_{\mathrm{RP}}\}/\epsilon_2\{\psi_{\mathrm{PP}}\} \approx a^{\mathrm{PP}} ,$$

$$a^{\mathrm{PP}}_{B_{\mathrm{sq}}} \equiv B_{\mathrm{sq}}\{\psi_{\mathrm{PP}}\}/B_{\mathrm{sq}}\{\psi_{\mathrm{RP}}\} \approx a^{\mathrm{PP}} .$$

where $a^{\mathrm{PP}} \equiv \langle \cos 2(\psi_{\mathrm{PP}} - \psi_{\mathrm{RP}})\rangle .$

$$a^{\mathrm{EP}}_{v_2} \equiv v_2\{\psi_{\mathrm{RP}}\}/v_2\{\psi_{\mathrm{EP}}\} \approx a^{\mathrm{EP}} ,$$

$$a^{\mathrm{EP}}_{B_{\mathrm{sq}}} \equiv B_{\mathrm{sq}}\{\psi_{\mathrm{EP}}\}/B_{\mathrm{sq}}\{\psi_{\mathrm{RP}}\} \approx a^{\mathrm{EP}} .$$

where $a^{\mathrm{EP}} = \langle \cos 2(\psi_{\mathrm{EP}} - \psi_{\mathrm{RP}})\rangle/\mathcal{R}_{\mathrm{EP}}$

EM filed

$$e\mathbf{B}(t,\mathbf{r}) = \frac{e^2}{4\pi}\sum_n Z_n(\mathbf{R}_n)\frac{1-v_n^2}{[R_n^2-(\mathbf{R}_n\times\mathbf{v}_n)^2]^{3/2}}\mathbf{v}_n\times\mathbf{R}_n,$$

$$e\mathbf{E}(t,\mathbf{r}) = \frac{e^2}{4\pi}\sum_n Z_n(\mathbf{R}_n)\frac{1-v_n^2}{[R_n^2-(\mathbf{R}_n\times\mathbf{v}_n)^2]^{3/2}}\mathbf{R}_n, \quad (2.1)$$

Eccentricity/elliptic flow

$$\epsilon_2\{\psi_{\{PP\}}\} = \langle \frac{\langle r_\perp^2 e^{2i\phi_r}\rangle}{\langle r_\perp^2\rangle}\rangle$$

$$v_2\{\psi_{\{EP\}}\} = \langle\langle e^{2i\phi}\rangle\rangle$$

CME-v_2 filter

CME and BKG are entangled in AA

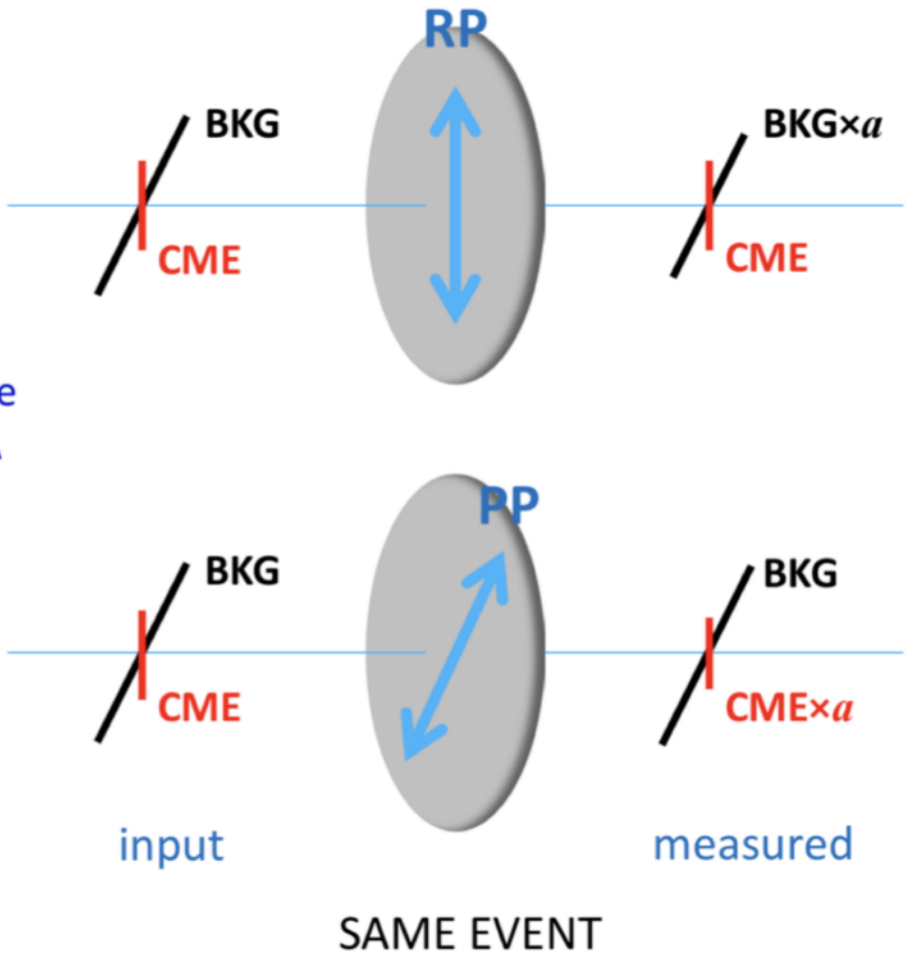

$$a \equiv \langle \cos 2(\psi_{PP} - \psi_{RP}) \rangle$$

Apply to data

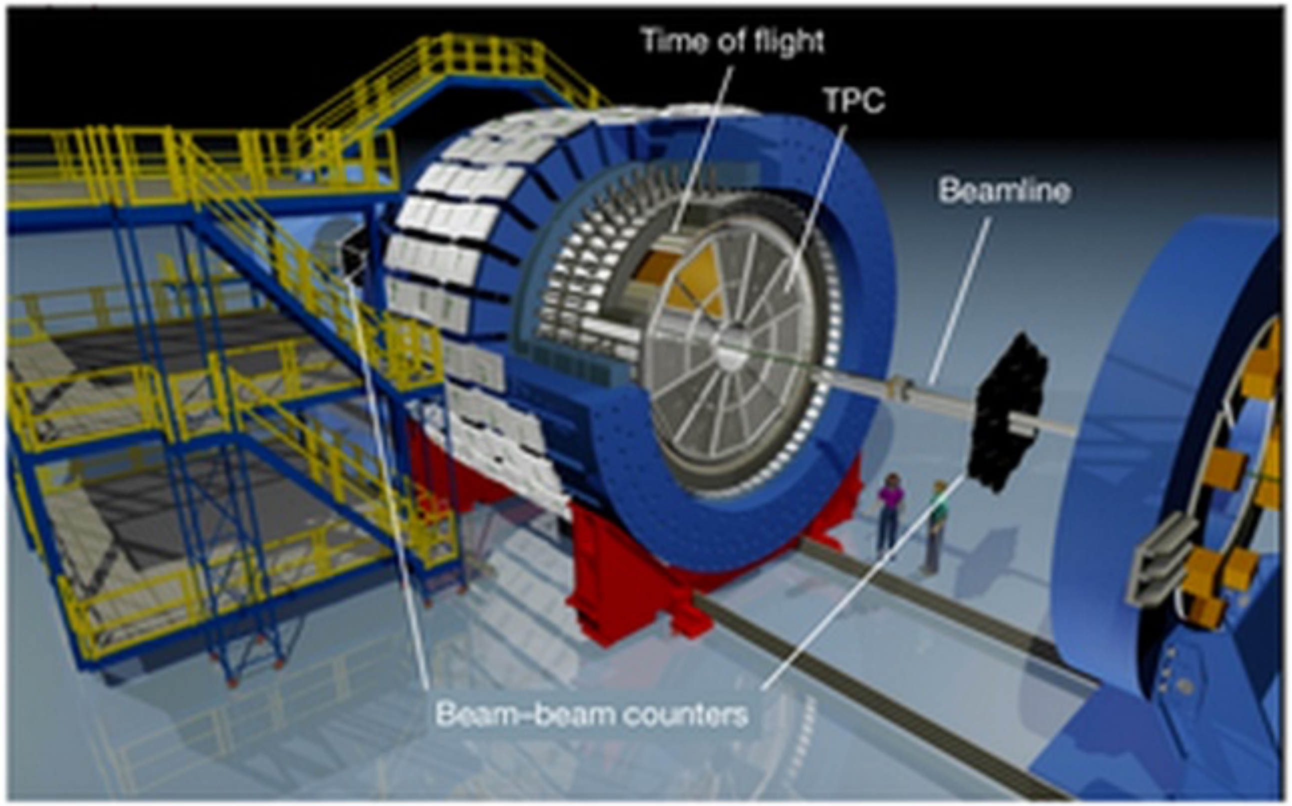

TPC: Ψ_{EP}, proxy of Ψ_{PP}
ZDC: Ψ_{ZDC}, proxy of Ψ_{SP} (Ψ_{RP})

$$f_{CME} = \frac{A/a - 1}{1/a^2 - 1}$$

where

$$A = \Delta\gamma_{ZDC}/\Delta\gamma_{TPC}$$

$$a = v_2\{ZDC\}/v_2\{TPC\}$$

STAR AuAu@200GeV

STAR, PRL128, 092301 (2022)

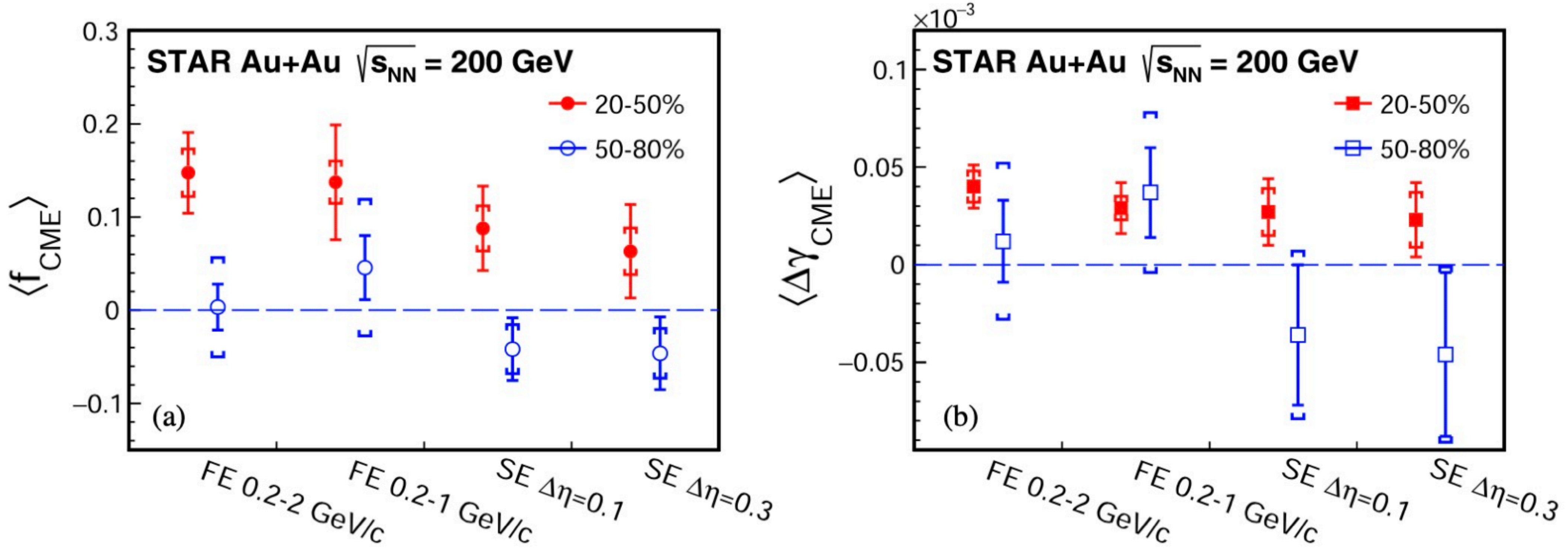

Indications of finite signal in mid-central 20-50% collisions, with 1-3σ significance (2.4B)

Expect 20B events from Run23 + Run25.

Non-flow effect

Y. Feng, et.al, PRC105, 024913 (2022)

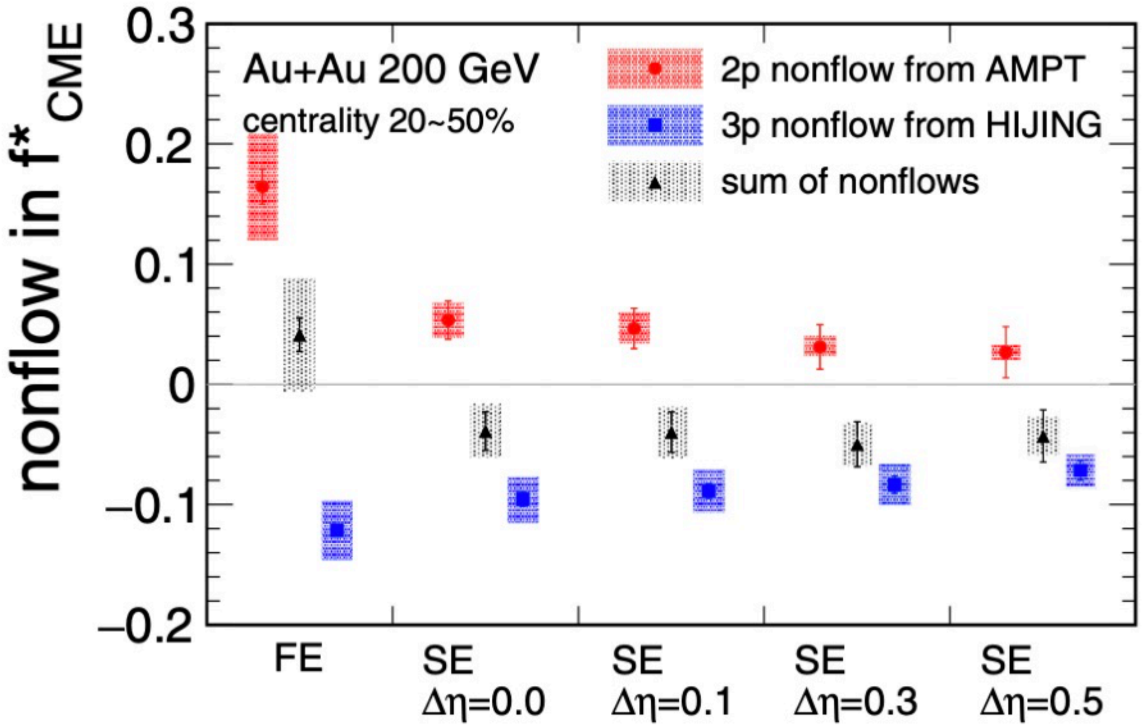

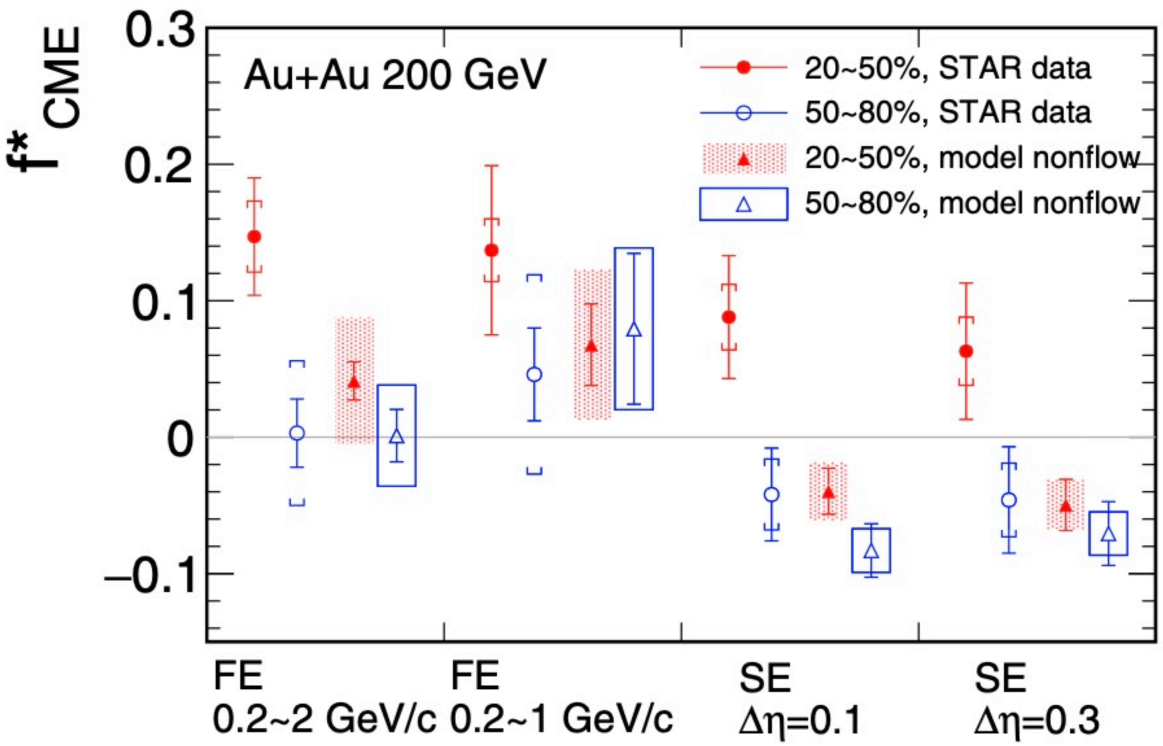

Need more rigorous non-flow studies

III. Search for the CME with Relativistic isobar collisions

Relativistic isobaric collisions

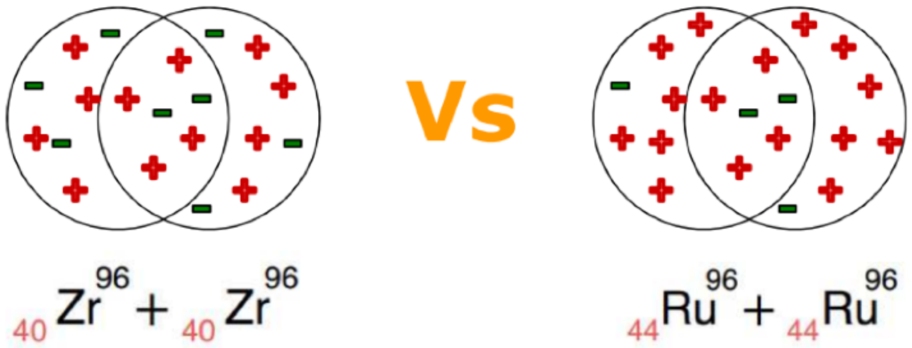

- Same multiplicity distributions, eccentricities => same background
- Different magnetic field => different CME signals

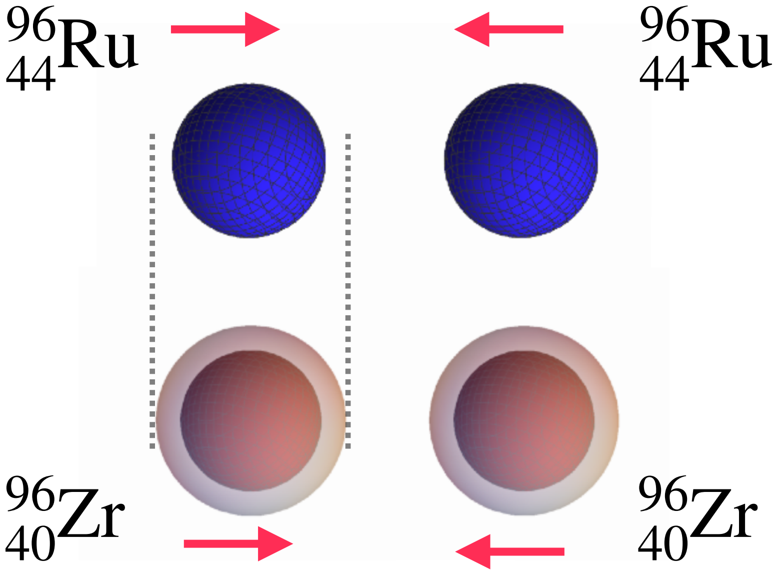

Isobar structure difference

Relativistic isobaric collisions and chiral magnetic effect

	R	a	beta2
Zr	5.02	0.46	0.08/0.217
Ru	5.085	0.46	0.158/0.053

WS parameters extracted from charge density distributions W. Deng, X. Huang, et.al., PRC94,041901(2016)

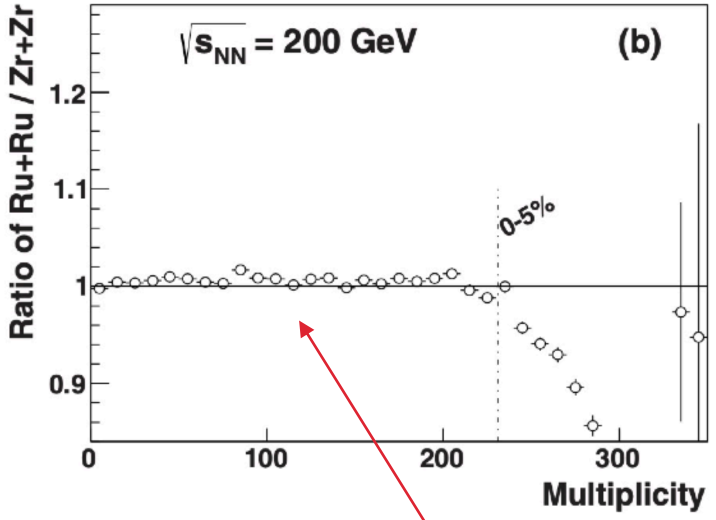

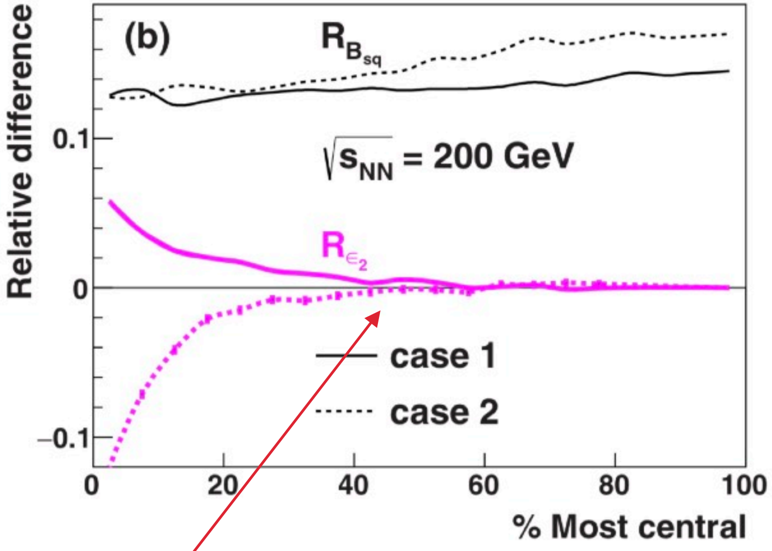

$$\Delta\gamma_{bkg} = \langle\cos(\varphi_\alpha + \varphi_\beta - 2\Psi_{RP})\rangle = \frac{N_{cluster}}{N_\alpha N_\beta} \times \langle\cos(\varphi_\alpha + \varphi_\beta - 2\Psi_{cluster})\rangle \times v_{2,cluster}$$

Isobar structures are important for the CME search

STAR, Isobar, PRC105, 014901(2022)

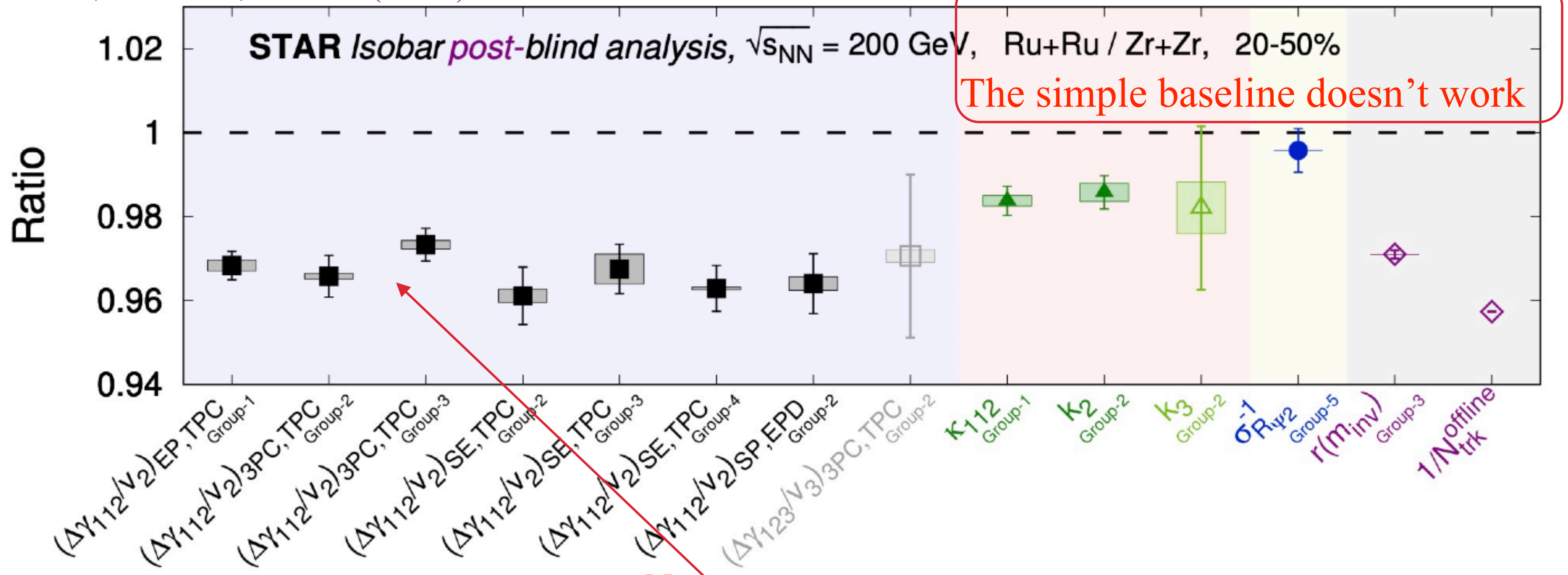

$$\Delta\gamma_{\rm bkg} = \langle\cos(\varphi_\alpha+\varphi_\beta-2\Psi_{RP})\rangle = \frac{N_{\rm cluster}}{N_\alpha N_\beta}\times\langle\cos(\varphi_\alpha+\varphi_\beta-2\Psi_{\rm cluster})\rangle\times v_{2,\rm cluster}$$

Multiplicity differences

Flow differences

The multiplicity and v2 differences from isobar structure are crucial for the CME search in the isobar collisions at RHIC

Neutron skin and symmetry energy

Charge density ≠ nuclear density.

Nuclear density distribution:

- Proton distribution — Can be accurately measured in experiment.
- Neutron distribution — Poorly known

Neutron skin: RMS radii differences between neutron distribution and proton distribution

$$\Delta r_{np} \equiv \sqrt{\langle r_n^2 \rangle} - \sqrt{\langle r_p^2 \rangle}$$

Neutron skin depends on symmetry energy:

$$E(\rho, \delta) = E_0(\rho) + E_{\mathrm{sym}}(\rho)\delta^2 + O(\delta^4)$$

$$\rho = \rho_n + \rho_p; \ \delta = \frac{\rho_n - \rho_p}{\rho}$$

$$L(\rho_c) = 3\rho_c \left[\frac{dE_{\mathrm{sym}}(\rho)}{d\rho} \right]_{\rho=\rho_c} ; \ \rho_c \simeq 0.11\mathrm{fm}^{-3}$$

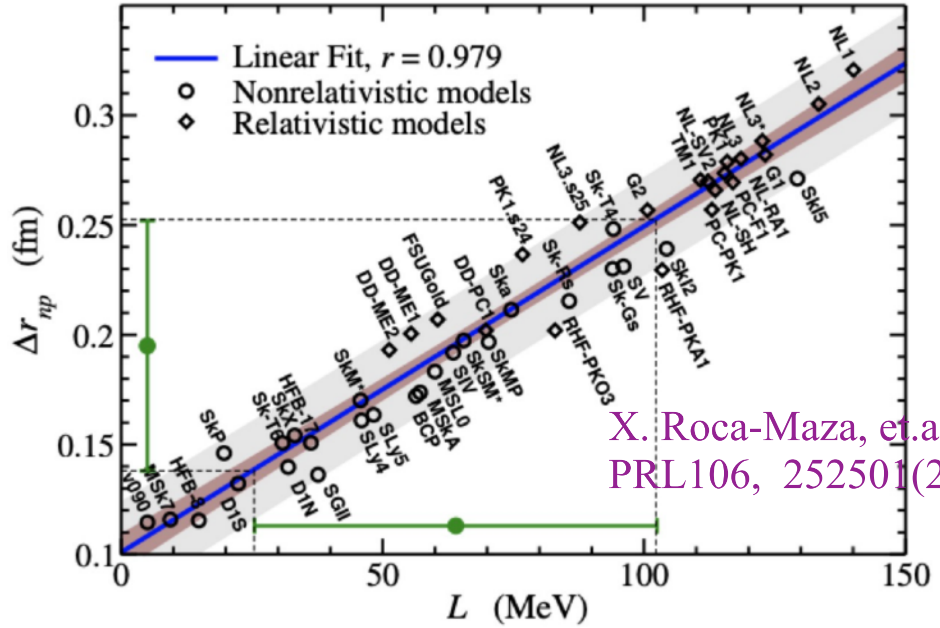

X. Roca-Maza, et.al., PRL106, 252501(2011)

The symmetry energy is crucial to our understanding of the masses and drip lines of neutron-rich nuclei and the equation of state (EOS) of nuclear and neutron star matter.

Charge densities and nuclear density in isobar collisions

HJX, et.al., PRL121, 022301 (2018)
H. Li, HJX, et.al., PRC98, 054907(2018)

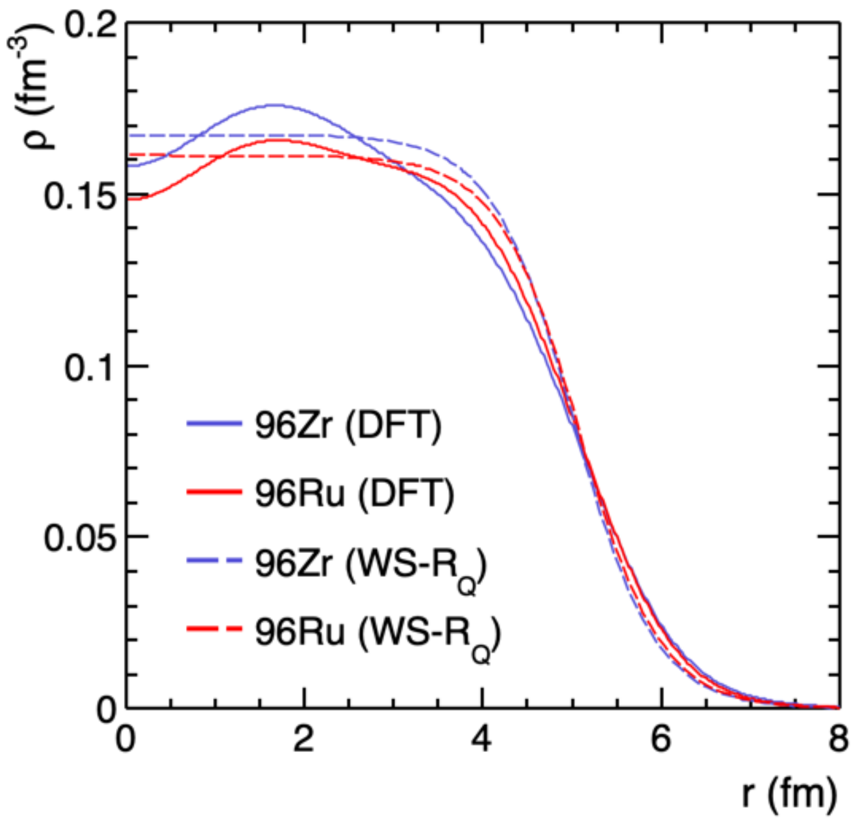

- Instead of the WS densities with parameters extracted from the measured charge densities, we use the proton and neutron densities obtained from the energy density functional theory (DFT) with Skyrme parameter set SLy4.

Multiplicity distribution difference between isobars

Predictions with charge densities

W. Deng, et.al., PRC94,041901(2016)

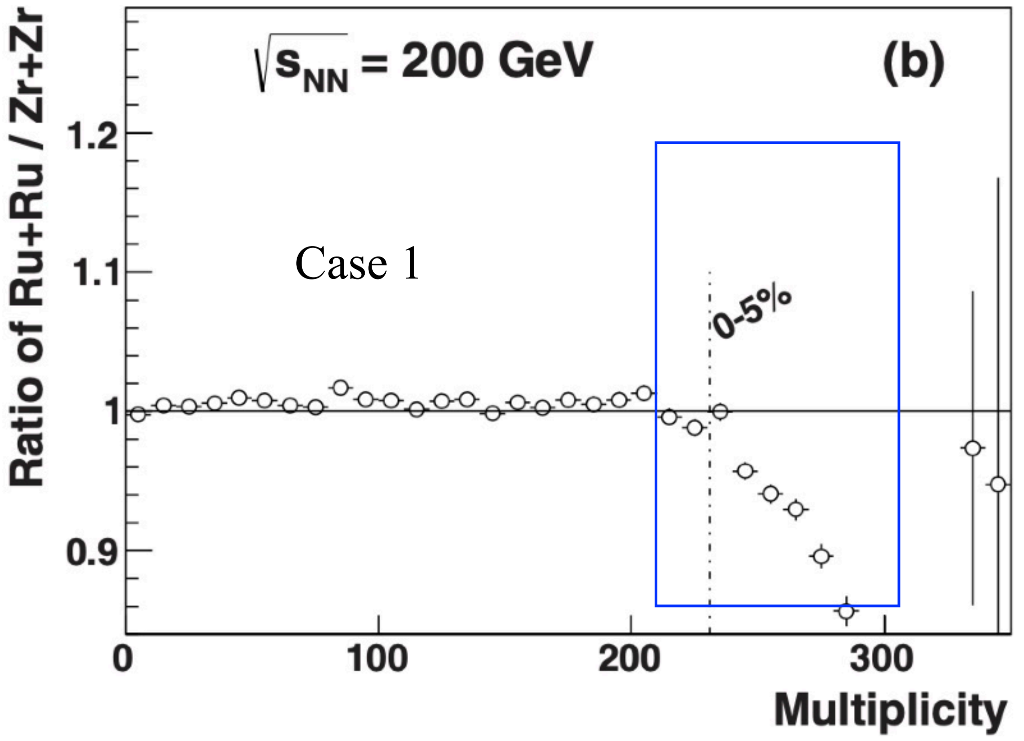

Predictions with DFT densities

H. Li, HJX, et.al., PRC98, 054907(2018)

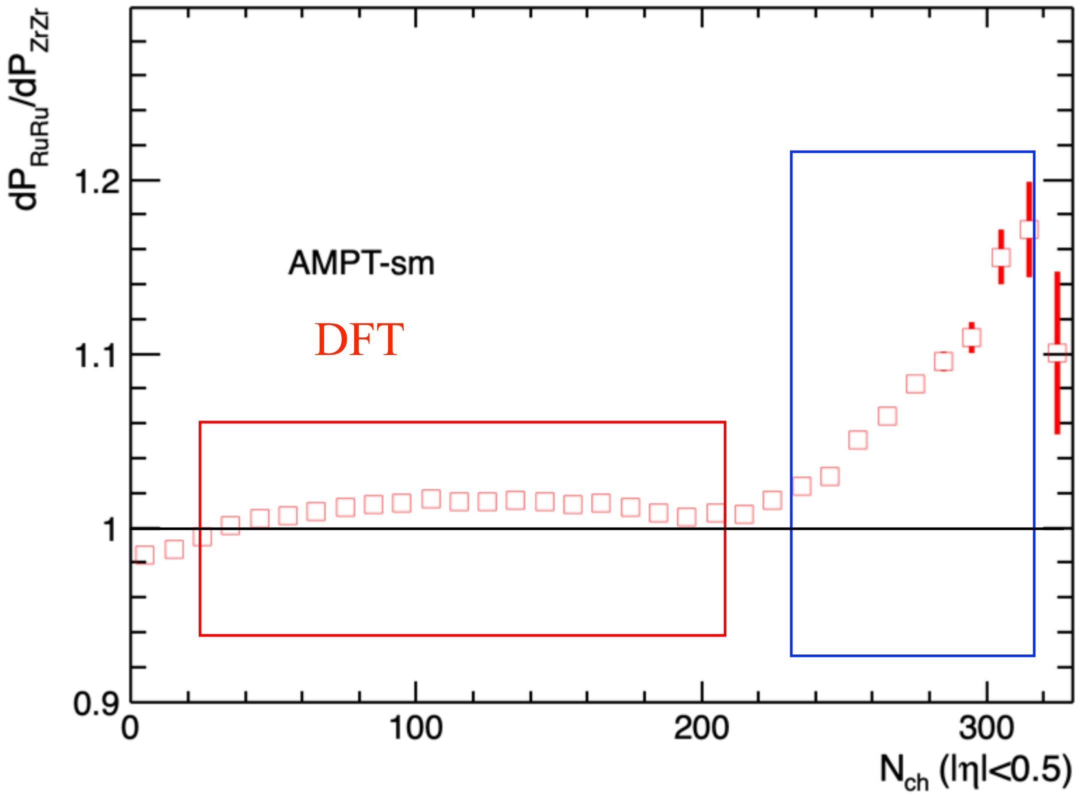

Opposite predictions from WS charge densities and DFT densities (neutron skins)

v_2 difference between isobars

Predictions from charge densities with deformation

W. Deng, et.al., PRC94,041901(2016)

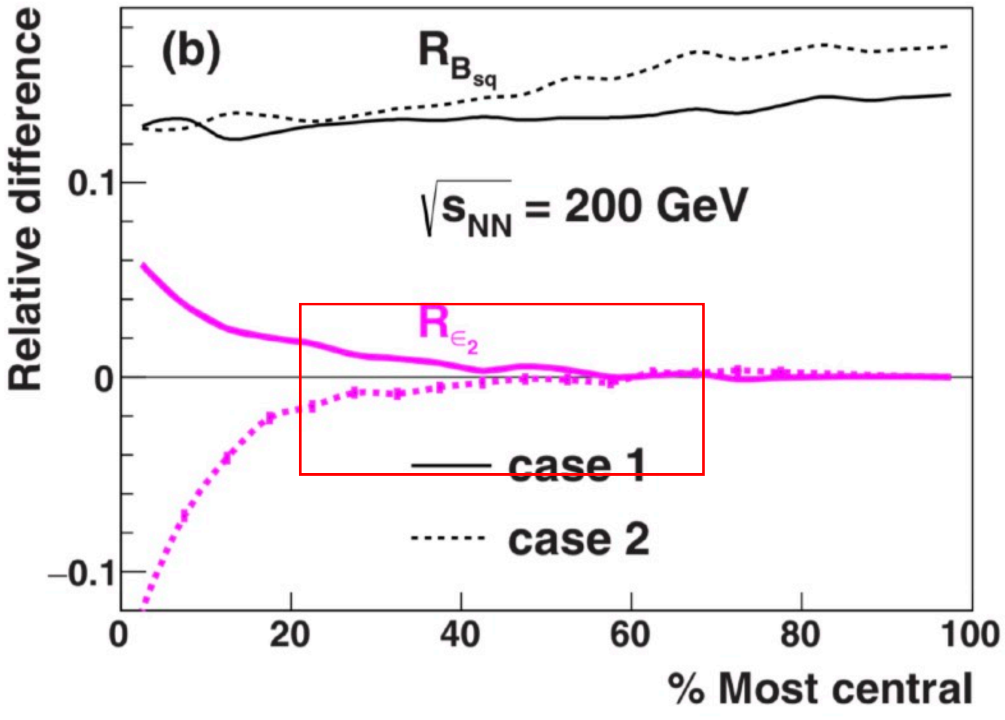

Predictions from DFT densities without deformation

HJX, et.al., PRL121, 022301 (2018)

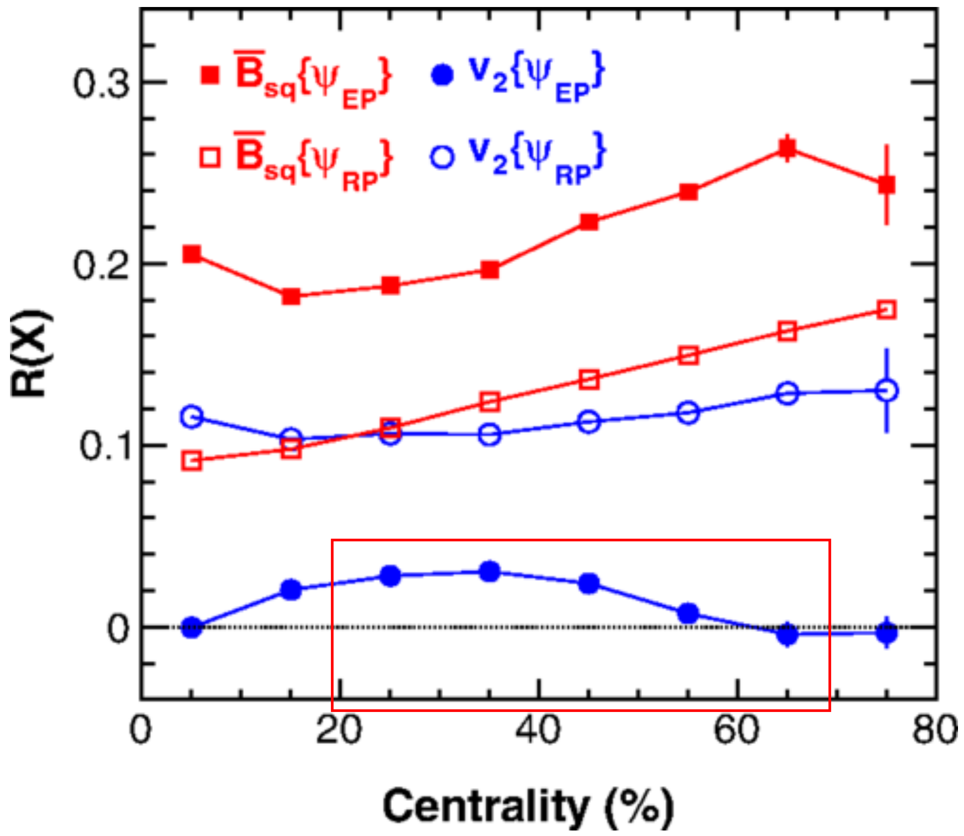

Compare to the predictions from charge densities, the calculations with DFT densities indicate that the Zr+Zr collisions and Ru+Ru collisions **have sizable differences in v_2 in 20-50% centrality range**.

Haojie Xu

Determine the neutron skin type by STAR data

HJX, et.al., PLB819, 136453 (2021)

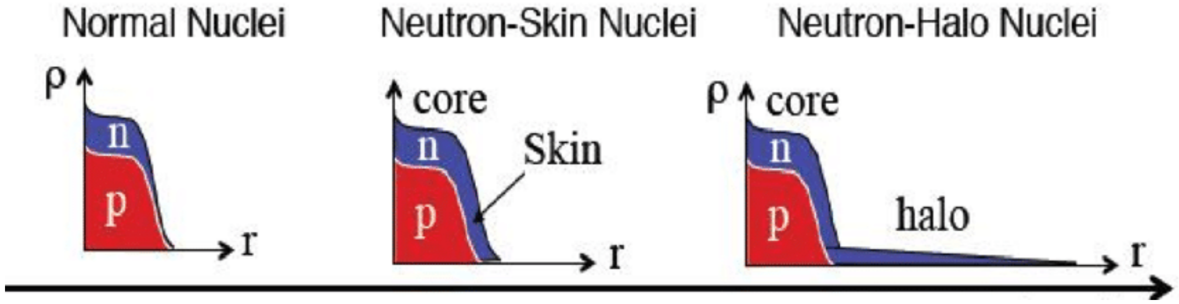

- Neutron-skin nuclei and neutron-halo nuclei for Zr

	^{96}Ru		^{96}Zr	
	R	*a*	*R*	*a*
p	5.085	0.523	5.021	0.523
skin-type n	5.085	0.523	5.194	0.523
halo-type n	5.085	0.523	5.021	0.592

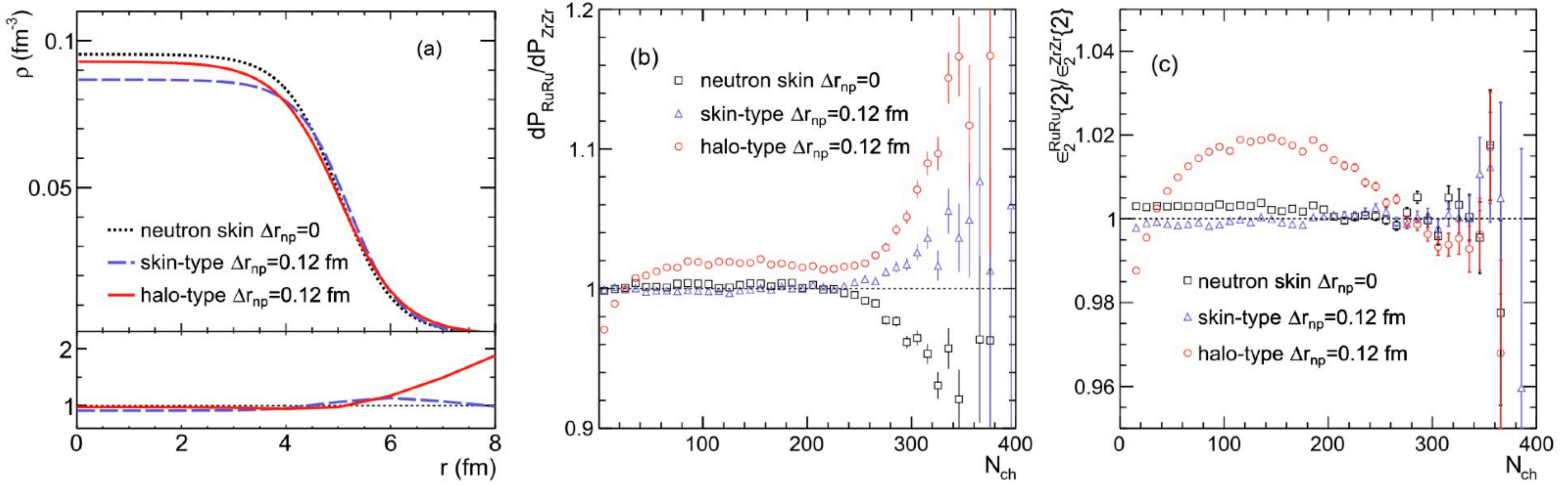

The shapes of the Ru+Ru/Zr+Zr ratios of the multiplicity and eccentricity in mid-central collisions can further distinguish between skin-type and halo-type neutron densities.

DFT predictions are “verified” by STAR data

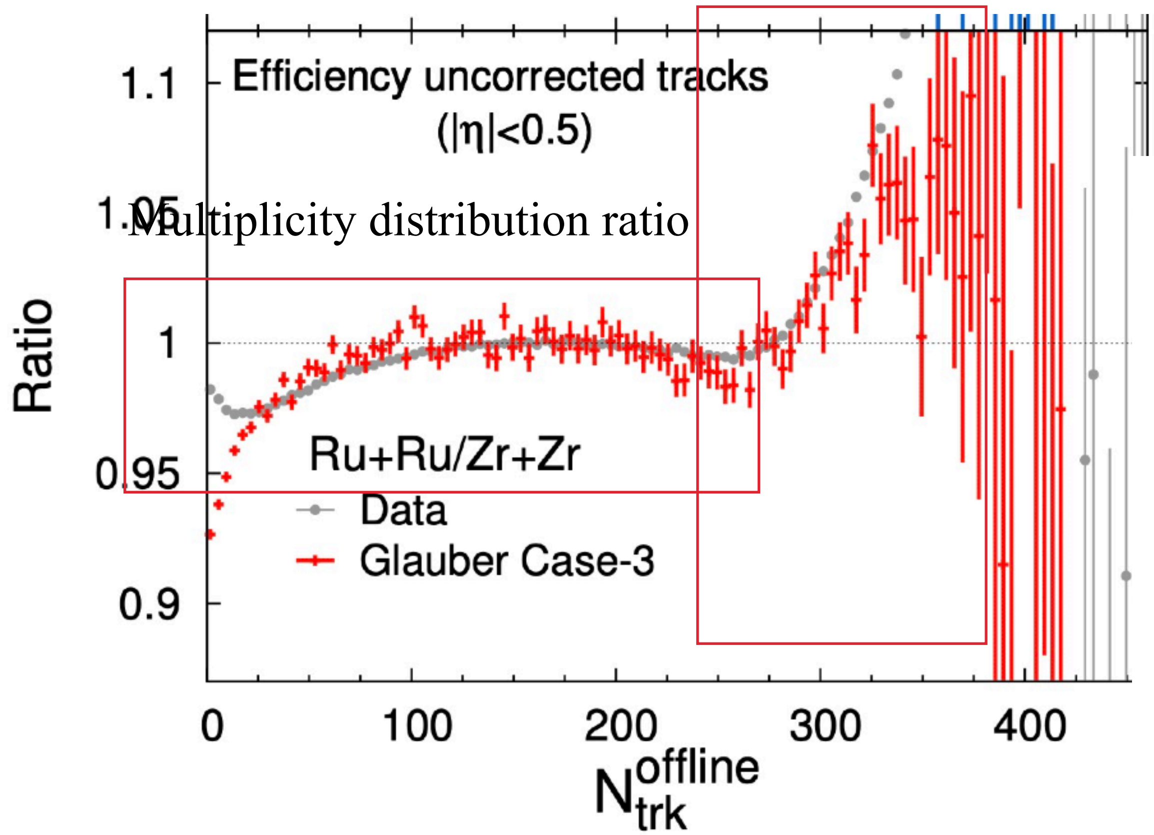

STAR, PRC105, 014901(2022)

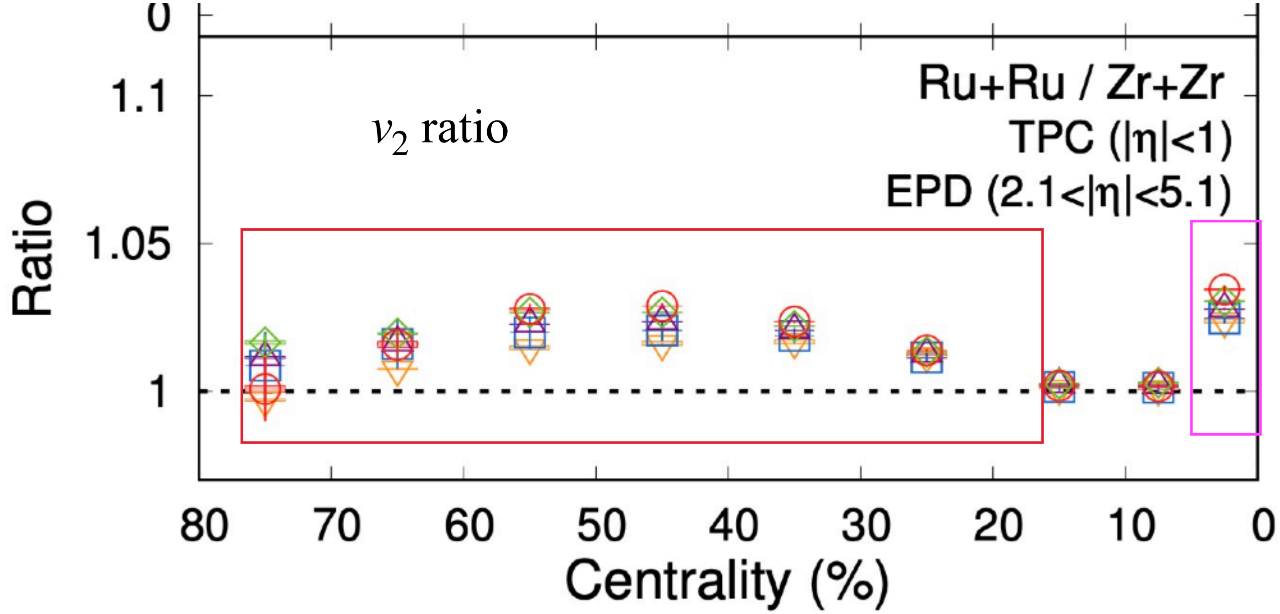

- STAR data indicate a thick neutron skin for the Zr nuclei, consistent with DFT predictions
- STAR data indicate a halo-type neutron skin, also consistent with DFT predictions

Isobar structures are important for the CME search

Y. Feng [STAR], SQM2022

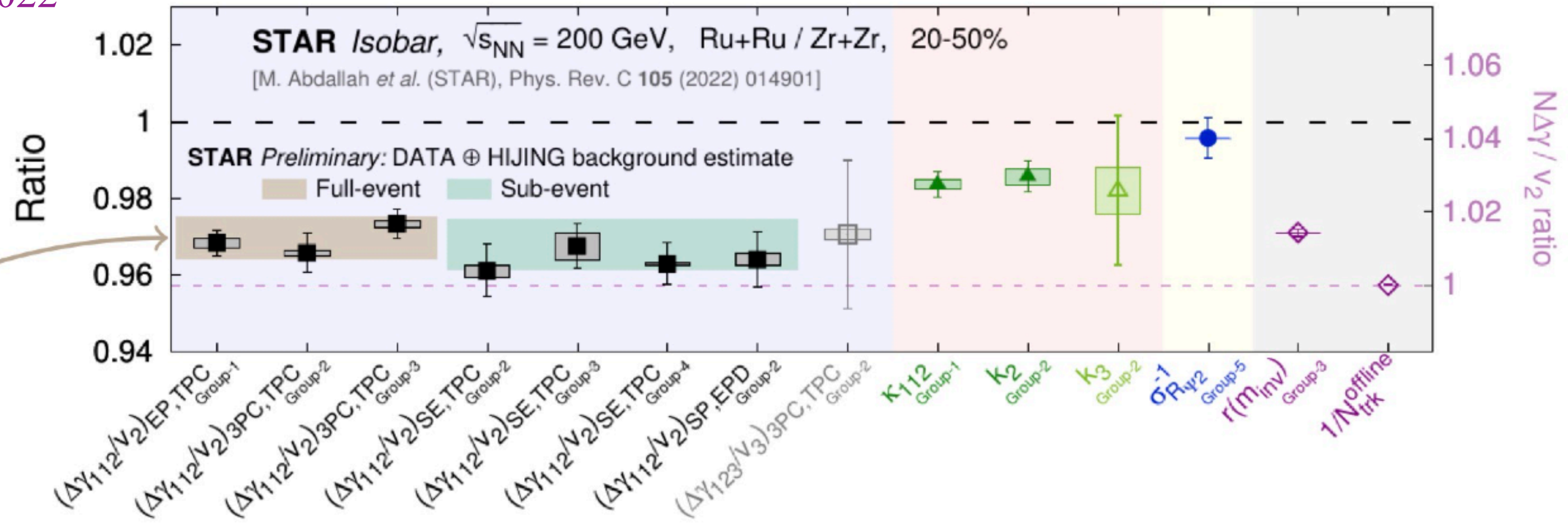

$$\frac{(N\Delta\gamma/v_2^*)^{\mathrm{Ru}}}{(N\Delta\gamma/v_2^*)^{\mathrm{Zr}}} \approx 1+\frac{\Delta\epsilon_2}{\epsilon_2}-\frac{\Delta\epsilon_{\mathrm{nf}}}{1+\epsilon_{\mathrm{nf}}}+\frac{\epsilon_3/\epsilon_2/(Nv_2^2)}{1+\epsilon_3/\epsilon_2/(Nv_2^2)}\left(\frac{\Delta\epsilon_3}{\epsilon_3}-\frac{\Delta\epsilon_2}{\epsilon_2}-\frac{\Delta N}{N}-\frac{\Delta v_2^2}{v_2^2}\right)$$

$$=1+(1.45\pm0.08)\%+(0.65\pm0.11\pm0.22)\%$$

$$+(0.094\pm0.007\pm0.048)\left[(0.5\pm2.7)\%-(1.45\pm0.08)\%-4.4\%-(3.7\pm0.1\pm0.3)\%\right]$$

$$=1+(1.45\pm0.08)\%+(0.65\pm0.11\pm0.22)\%-(0.85\pm0.26\pm0.44)\%$$

$$=\mathbf{1.013\pm0.003\pm0.005} \quad \text{(full-event)}$$

IV. Probing the neutron structure with relativistic isobaric collisions

Current status of neutron skin measurements

PREX-2 Collaboration, PRL126, 172502(2021); B. Reed, et.al., PRL126, 172503(2021)

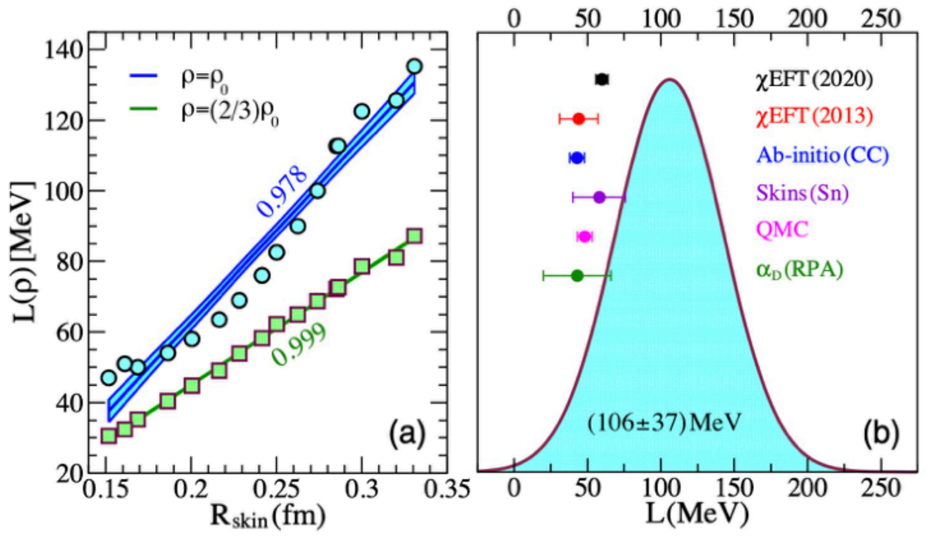

FIG. 1. Left: slope of the symmetry energy at nuclear saturation density ρ_0 (blue upper line) and at $(2/3)\rho_0$ (green lower line) as a function of $R^{208}_{\rm skin}$. The numbers next to the lines denote values for the correlation coefficients. Right: Gaussian probability distribution for the slope of the symmetry energy $L = L(\rho_0)$ inferred by combining the linear correlation in the left figure with the recently reported PREX-2 limit. The six error bars are constraints on L obtained by using different theoretical approaches [14,19–25].

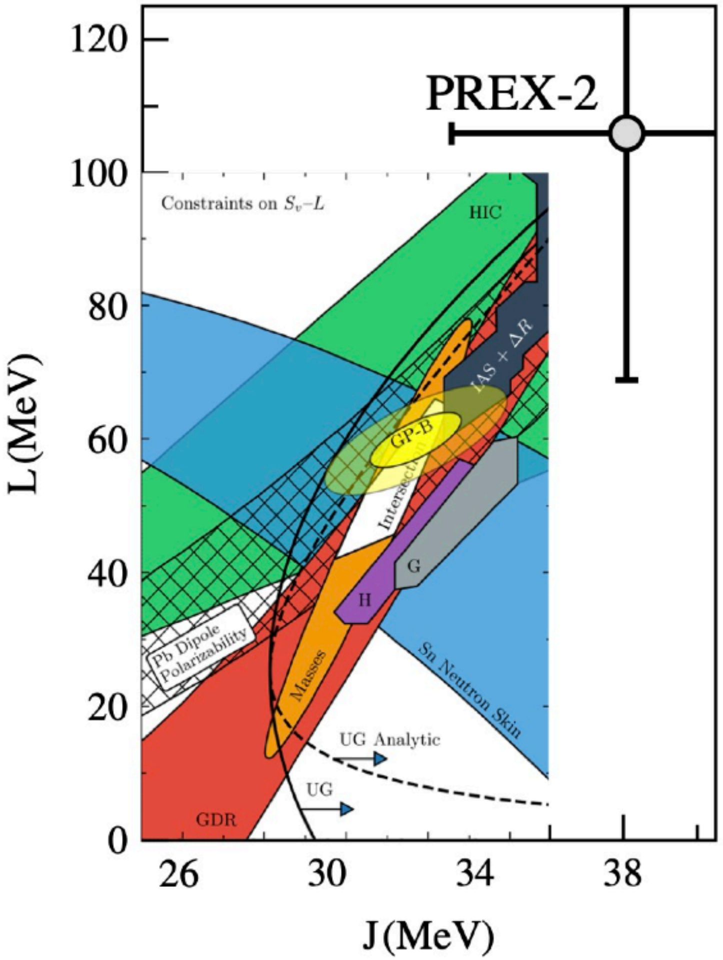

$$\Delta r_{\rm np}^{\rm Pb} = (0.284 \pm 0.071)\ {\rm fm}$$

$$L(\rho_0) = (106 \pm 37)\ {\rm MeV}$$

$$L(\rho_c) = (71.5 \pm 22.6)\ {\rm MeV}$$

This PREX-2 result favors a large neutron skin thickness and symmetry energy slope parameter, at tension with existing experimental data and theoretical analyses.

Neutron skin and nuclear symmetry energy

H. Li, HJX, et.al., PRL125, 222301(2020)

SHF: Standard Skyrme-Hartree-Fock (SHF) model
eSHF: Extended SHF model

$$E(\rho,\delta) = E_0(\rho) + E_{\rm sym}(\rho)\delta^2 + O(\delta^4)$$

$$\rho = \rho_n + \rho_p;\ \delta = \frac{\rho_n - \rho_p}{\rho}$$

$$L(\rho_c) = 3\rho_c \left[\frac{dE_{\rm sym}(\rho)}{d\rho}\right]_{\rho=\rho_c};\ \rho_c \simeq 0.11 {\rm fm}^{-3}$$

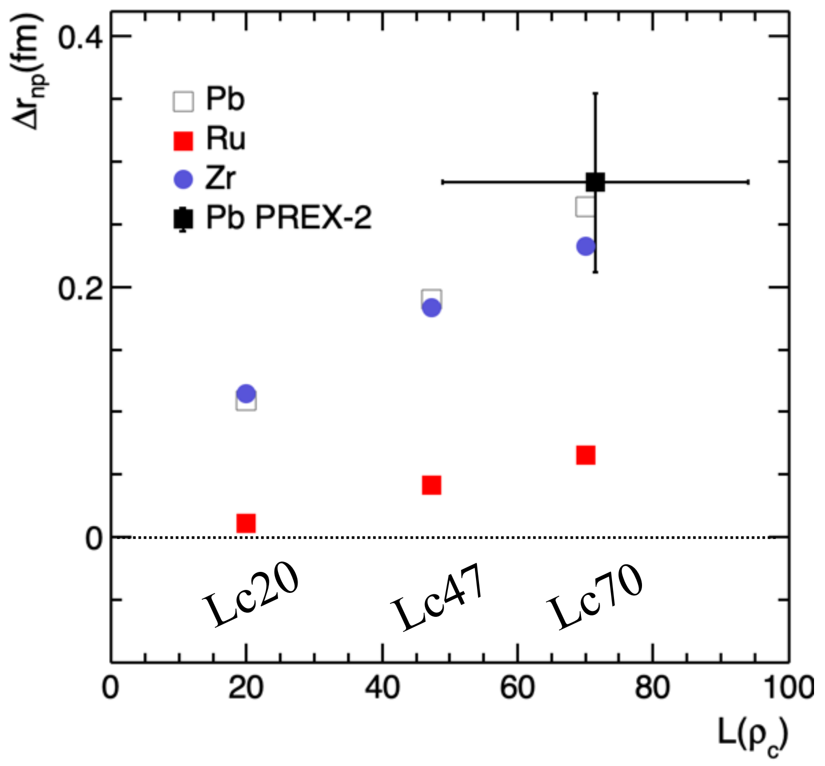

Z. Zhang, PRC94, 064326(2016)

$$\begin{aligned} v_{i,j} &= t_0(1+x_0P_\sigma)\delta(\boldsymbol{r}) + \frac{1}{6}t_3(1+x_3P_\sigma)\rho^\alpha(\boldsymbol{R})\delta(\boldsymbol{r}) \\ &+ \frac{1}{2}t_1(1+x_1P_\sigma)[K'^2\delta(\boldsymbol{r}) + \delta(\boldsymbol{r})K^2] \\ &+ t_2(1+x_2P_\sigma)\boldsymbol{K}'\cdot\delta(\boldsymbol{r})\boldsymbol{K} \\ &+ \frac{1}{2}t_4(1+x_4P_\sigma)[K'^2\delta(\boldsymbol{r})\rho(\boldsymbol{R}) + \rho(\boldsymbol{R})\delta(\boldsymbol{r})K^2] \\ &+ t_5(1+x_5P_\sigma)\boldsymbol{K}'\cdot\rho(\boldsymbol{R})\delta(\boldsymbol{r})\boldsymbol{K} \\ &+ iW_0(\boldsymbol{\sigma}_i+\boldsymbol{\sigma}_j)\cdot[\boldsymbol{K}'\times\delta(\boldsymbol{r})\boldsymbol{K}], \end{aligned} \quad (4)$$

Extended

			^{96}Zr			^{96}Ru			^{208}Pb
	$L(\rho_c)$	$L(\rho_0)$	r_n	r_p	$\Delta r_{\rm np}$	r_n	r_p	$\Delta r_{\rm np}$	$\Delta r_{\rm np}$
Lc20	20	13.1	4.386	4.27	0.115	4.327	4.316	0.011	0.109
Lc47	47.3	55.7	4.449	4.267	0.183	4.360	4.319	0.042	0.190
Lc70	70	90.0	4.494	4.262	0.232	4.385	4.32	0.066	0.264
SLy4	42.7	46.0	4.432	4.271	0.161	4.356	4.327	0.030	0.160

Method I: multiplicity distribution ratio

H. Li, HJX, et.al., PRL125, 222301(2020)

Lc47: DFT calculations using data from terrestrial nuclear experiments and astrophysical observations. Y. Zhou, L. Chen, Z. Zhang, PRD99, 121301R(2021)

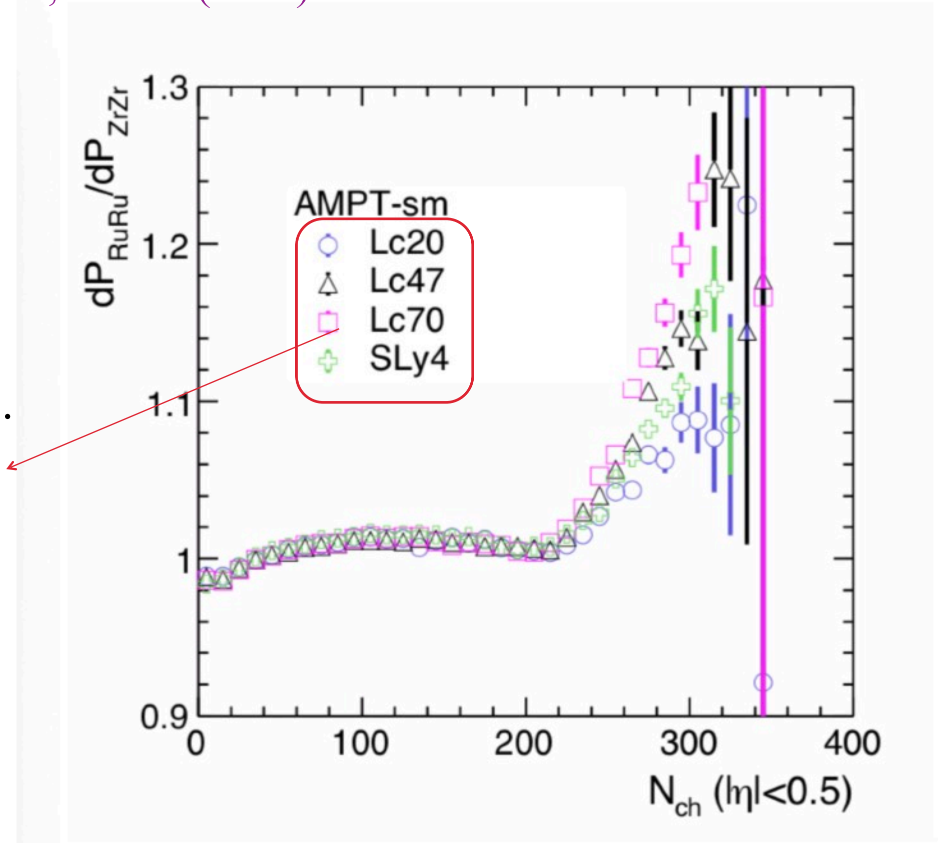

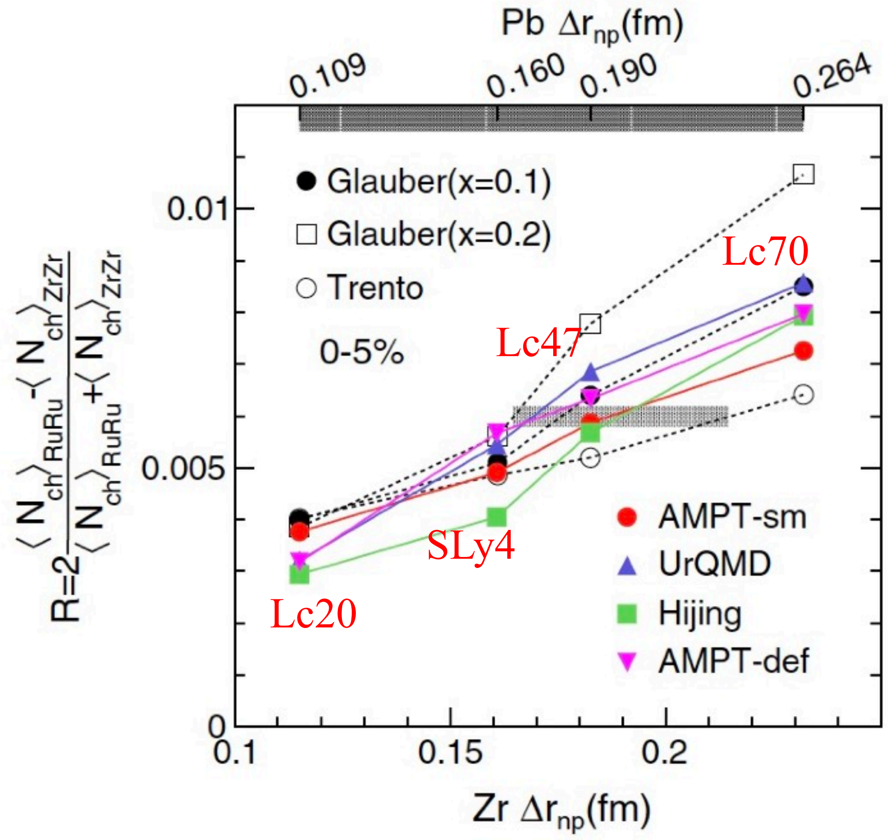

- The ratio of N_{ch} distributions highlight the differences
- To quantify the differences, we use the R observable of N_{ch} at top 5% centrality.
- R is a relative measure, **much of experimental effects cancel**
- Deformation has an effect on the tail. Quantitative investigation underway.

Method II: mean p_T ratio

HJX, et.al, arXiv:2111.14812

b=0 fm

A → smaller $R_\perp$ → larger N_{ch} and $\langle p_T\rangle$

B → Larger $R_\perp$ → Smaller N_{ch} and $\langle p_T\rangle$)

$$R(\langle p_T\rangle) \propto R(d_\perp) \propto 1/R(\langle\sqrt{r^2}\rangle)$$

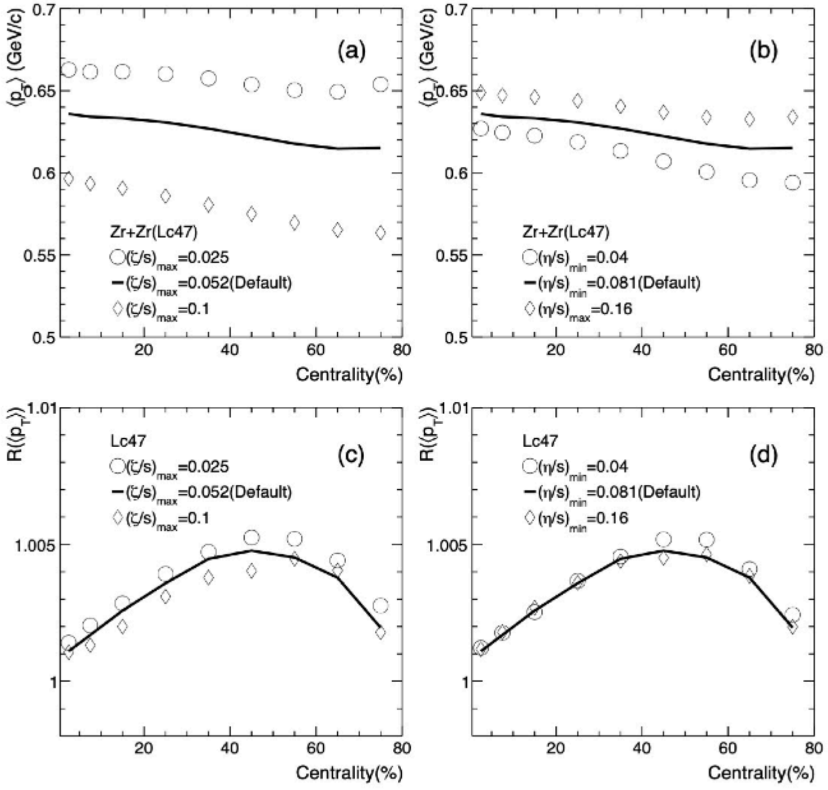

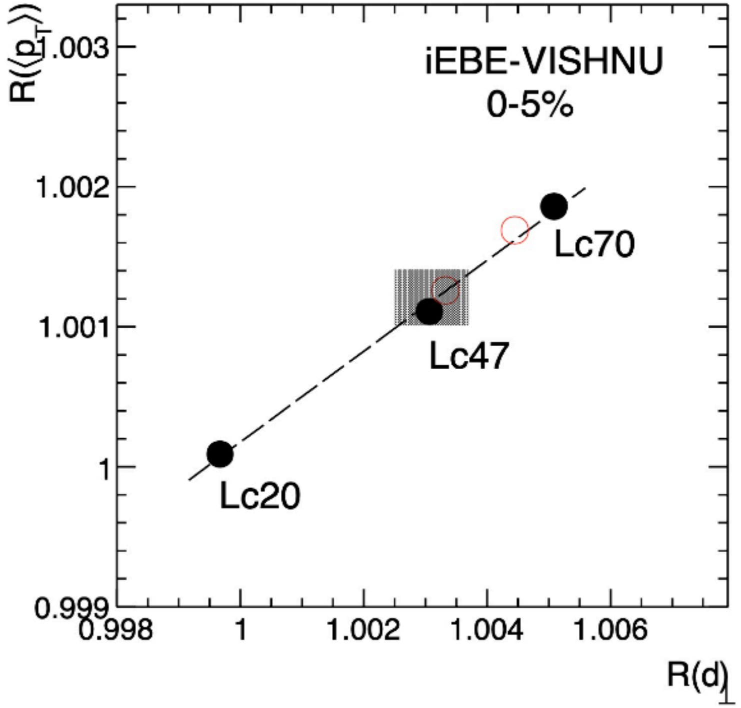

The $R(\langle p_T\rangle)$ is inversely proportional to nuclear size ratio in most central collisions.

Method III: net-charge ratio in very peripheral collisions

HJX, et.al., PRC105, L011901 (2022)

For the colliding nuclei with large neutron skin thickness

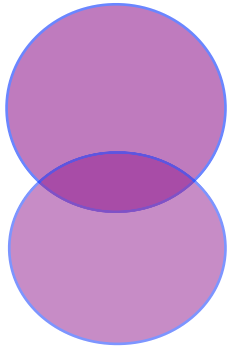

→ more n+n collisions at most peripheral collisions → Less participant charges, thus less final net-charges

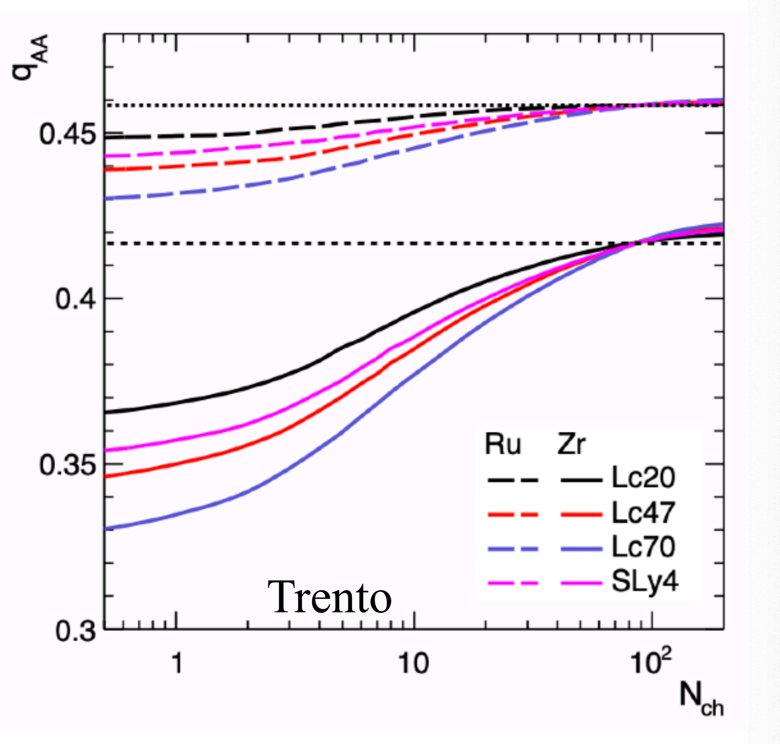

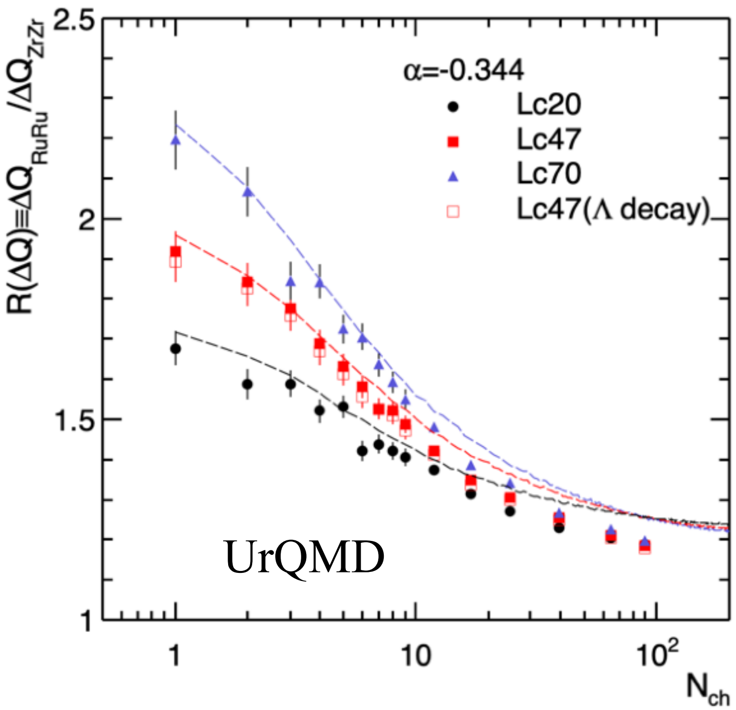

The curves are calculated by superimposition assumption

$$R(\Delta Q) = \frac{q_{RuRu} + \alpha/(1-\alpha)}{q_{ZrZr} + \alpha/(1-\alpha)}$$

where $q_{RuRu/ZrZr}$ are the fraction of protons among the participant nucleons, obtained by the Trento model.

α is the ΔQ ratio in nn to pp interaction:

Pytha: $\alpha = -0.352$

Hijing: $\alpha = -0.389$

UrQMD: $\alpha = -0.344$

Haojie Xu

STAR measurements

HJX(STAR), QM2022

18

Compare to world wide data

State-of-the-art **spherical** DFT with eSHF nuclear potential

Zhang, Chen, PRC94, 064326 (2016)

- Multiplicity ratio:

  $L(\rho_c) = 53.8 \pm 1.7 \pm 7.8$ MeV

  $L(\rho) = 65.4 \pm 2.1 \pm 12.1$ MeV

  $\Delta r_{\mathrm{np,Zr}} = 0.195 \pm 0.019$ fm

  $\Delta r_{\mathrm{np,Ru}} = 0.051 \pm 0.009$ fm

- $\langle p_T \rangle$ ratio:

  $L(\rho_c) = 56.8 \pm 0.4 \pm 10.4$ MeV

  $L(\rho) = 69.8 \pm 0.7 \pm 16.0$ MeV

  $\Delta r_{\mathrm{np,Zr}} = 0.202 \pm 0.024$ fm

  $\Delta r_{\mathrm{np,Ru}} = 0.052 \pm 0.012$ fm

B. Li, et.al Universe 7, 182 (2021)

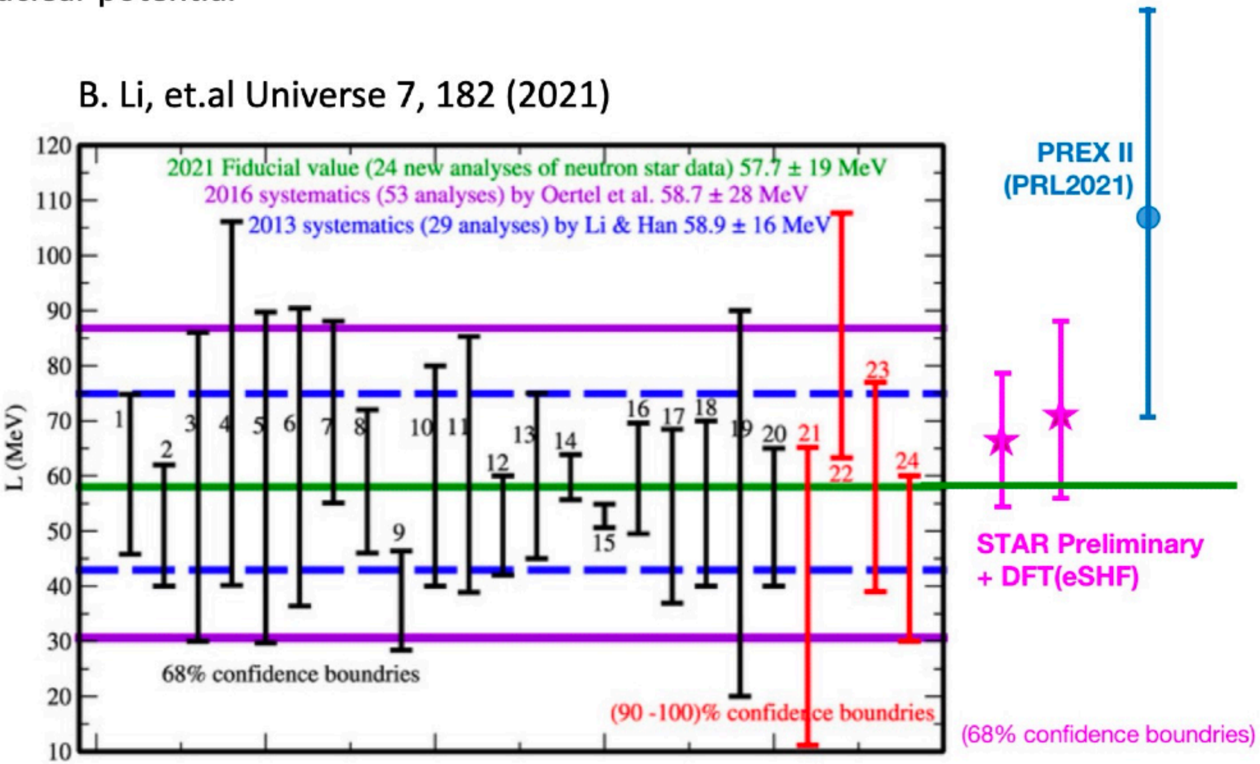

Consistent with world wide data with good precision

V. SUMMARY

- Although current data are too weak to be definitive, the SP/PP method points out a potentially very important direction for CME search.
- The isobar density distributions are **crucial for the CME search**.
  - Sizable v_2 and multiplicity distribution differences at non-central collisions
  - Large enhancement of multiplicity differences and flow differences at most central collisions
- Ultra-relativistic isobar collisions can be used to **probe the isobar structure**, e.g. the neutron skin type, thickness, and nuclear deformation.
  - Multiplicity distribution ratio; Mean p_T ratio; Net charge ratio;
  - Flow observables, asymmetric cumulants

Thank you for your attention!

Haojie Xu(徐浩洁)

Huzhou University(湖州师范学院)